

1 **Damage to monumental masonry buildings in Hatay and Osmaniye following the 2023 Turkey earthquake sequence:**
2 **the role of wall geometry, construction quality and material properties**

3 Baran Bozyigit^{*1,2}, Anil Ozdemir³, Kokcan Donmez⁴, Korhan Deniz Dalgic⁵, Elif Durgut⁶, Cennet Yesilyurt⁵, Yavuz Dizgin⁷,
4 Canan Yildeniz⁸, Medine Ispir⁶, Idris Bedirhanoglu^{1,7}, Yasemin Didem Aktas⁴, Sinan Acikgoz¹

5
6 ¹Department of Engineering Science, University of Oxford, Oxford, UK

7 ²Department of Civil Engineering, Dokuz Eylul University, Izmir, Turkey

8 ³Department of Civil Engineering, Gazi University, Ankara, Turkey

9 ⁴Department of Civil, Environmental, and Geomatic Engineering, University College London, London, UK

10 ⁵Department of Civil Engineering, Izmir Institute of Technology, Urla, Izmir, Turkey

11 ⁶Department of Civil Engineering, Istanbul Technical University, Istanbul, Turkey

12 ⁷Department of Civil Engineering, Dicle University, Diyarbakir, Turkey

13 ⁸Chamber of Architects, Diyarbakir, Turkey

14
15 *Corresponding author: baran.bozyigit@deu.edu.tr

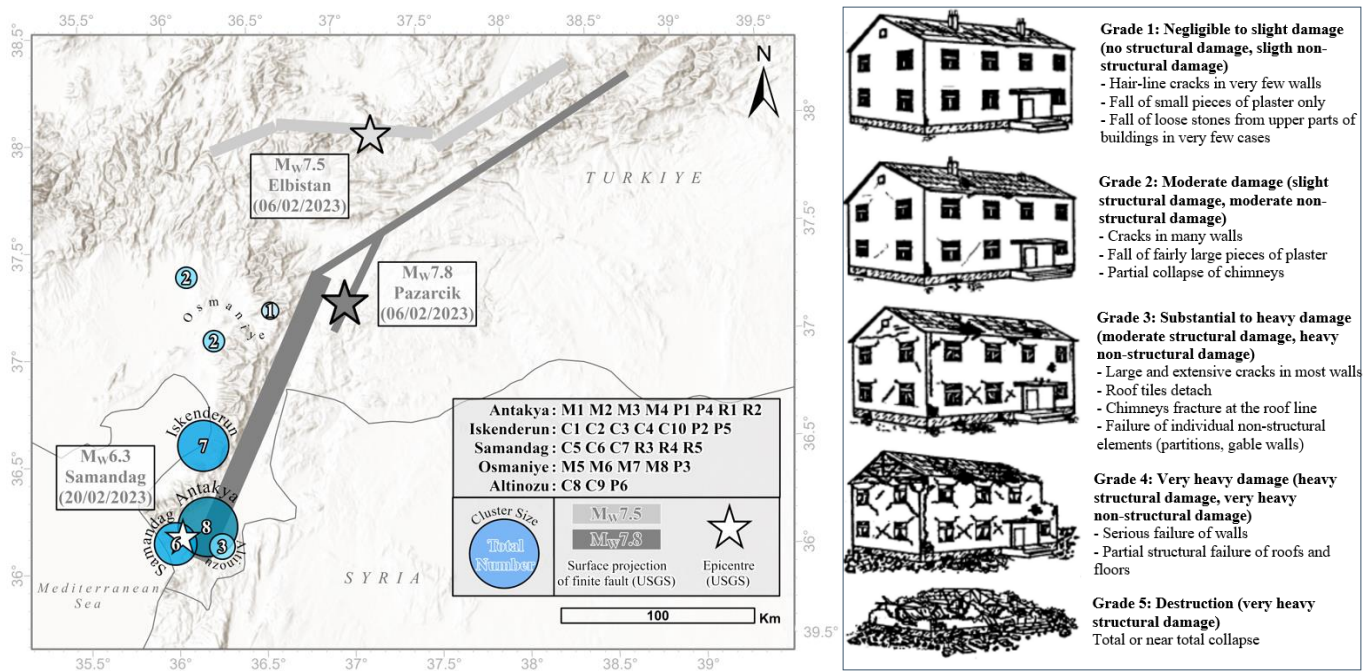
16
17 **Abstract** This paper reports on the findings of an investigation on 29 historic stone masonry buildings located in the cities of
18 Hatay and Osmaniye following the 2023 Turkey earthquake sequence. The earthquake couplet on 6 February (with moment
19 magnitudes 7.8 and 7.5) and the following events (including another earthquake which occurred on 20 February with a moment
20 magnitude of 6.3) resulted in significant damage to the buildings. To understand why, the examined buildings were assigned an
21 EMS-98 damage level (ranging from 1 to 5) and descriptive response categories (masonry disaggregation, local mechanism and
22 global response). Overall damage statistics indicated that masonry disaggregation was common and coterminous with local
23 mechanism response. Wall geometry and construction quality indices were then investigated to explore why these were the
24 dominant damage mechanisms. Wall geometry indices highlighted insufficient amount of walls to resist the local seismic
25 demands, particularly in the transverse (e.g. short) direction of buildings. This deficit promoted the formation of local
26 mechanisms. Construction quality indices suggested that stone layouts did not enable interlocking and that the walls were prone
27 to disaggregation. To further investigate the role of material properties on the observed damage, materials were characterised
28 using three non-destructive testing techniques: ultrasonic pulse velocity (UPV) measurements to estimate the static elastic
29 modulus of stones, Schmidt rebound hammer (SRH) tests to estimate the compressive strength of stones, and the mortar
30 penetrometer (MP) tests to estimate the compressive strength of mortar. The measurements indicated poor mortar quality, which
31 may have expedited failures. Using established correlations, various other important material parameters (e.g. mortar cohesion
32 and homogenised masonry strength) are derived. It is envisioned that the damage observations and the material measurements
33 in this paper will inform detailed modelling efforts on the behaviour of historic masonry buildings during the earthquakes.

34 **Keywords:** Masonry, Earthquake damage, Wall geometry index, Masonry quality index, Non-destructive testing, Mortar
35 penetrometer, Schmidt rebound hammer, Ultrasonic pulse velocity

36

37 **1. Introduction**

38 On 6 February 2023, at 04.17 and 13.24 (GMT+3 time zone), two earthquakes occurred in the province of Kahramanmaraş
 39 in Turkey. The first earthquake occurred at a depth of 10 km in Pazarcık and had a magnitude of $M_w=7.8$. The second earthquake
 40 occurred at a depth of 10 km in Elbistan and had a magnitude of $M_w=7.5$. Thousands of aftershocks followed in addition to
 41 earthquake on 20 February 2023, which had its epicentre in the Samandağ district of Hatay province. It occurred at a depth of
 42 16 km and had a magnitude of $M_w=6.3$ (USGS, 2023). More than 50.000 people have lost their lives and 212.000 buildings were
 43 severely damaged or collapsed in the affected provinces (Karabacak et al., 2023). Fig.1a highlights the epicentres of these
 44 earthquakes.



45
 46
 47 Fig.1. a) Distribution of investigated buildings (see Table 1 for building IDs) with epicentres of Pazarcık and Samandağ
 48 earthquakes b) graphical representation and damage classification of masonry buildings according to EMS-98 (Grünthal and
 49 Levret, 1998)

50 The historic urban environments in the provinces of Hatay and Osmaniye were severely affected. Iconic buildings of worship,
 51 such as the Habib-i Neccar Mosque (Sancı, 2006), partially collapsed during the earthquakes. Historic public buildings, built
 52 during the 20th century French mandate of Hatay (Garbioğlu, 2017), were in use as local government or school buildings before
 53 the earthquakes. These buildings sustained severe damage. The large vernacular masonry building stocks in the districts of
 54 Antakya (Demir, 2016) and Samandağ (Sürmeli, 2019) featured examples of unique local architectural practice. Many of these
 55 buildings collapsed.

56 The architectonic characteristics of specific religious, public and residential buildings were investigated in the
 57 aforementioned studies. However, these studies do not provide enough information on the construction practices and materials
 58 to carry out engineering assessments. During the early part of 2010s, a major research project called SERAMAR characterised

59 the general features of vernacular masonry building stock in Antakya (Abrahameczyk et al., 2013). This comprehensive study
60 included building surveys, material testing, building instrumentation, numerical modelling and risk mapping activities. However,
61 detailed data regarding some components of this research (e.g. material testing data) is not publicly available. Regardless,
62 amongst other contributions, the project highlighted observations regarding insufficient amount of walls and poor materials in
63 vernacular masonry constructions in the region (Geneş et al., 2017).

64 After the 2023 Turkey earthquake sequence, several reconnaissance reports and post-earthquake studies have been published.
65 Some of these reports emphasise the unique historical and architectural value of the historic structures in the region and present
66 visual observations of damage patterns (EERC, 2023; TAÇDAM, 2023). The reports also highlight the need to repair (and where
67 necessary strengthen) the monumental historic buildings that were damaged during the earthquakes. However, before the repair,
68 retrofit and reconstruction activities are carried out, it is necessary to conduct scientific studies to understand the general reasons
69 for damage. This paper presents an attempt to systematically categorise damage levels and types in monumental masonry
70 structures and relate it to their wall geometry, construction quality and material properties. To achieve this, damage observations
71 are quantified in Section 2. Section 3 and 4 investigate the potential role of geometric deficiencies (e.g. limited wall area) and
72 poor construction quality (e.g. lack of interlocking in walls) in causing the damage. To do this, wall geometry indices (Lourenço
73 et al., 2013) and masonry quality indices (Borri et al., 2015), are calculated for each building. Finally, Section 5 presents the
74 non-destructive measurements conducted to quantify the material properties in the historic buildings. The transformation of
75 damage observations, geometry, construction quality and material characteristics into quantifiable parameters enables a
76 systematic evaluation of the correlations between these aspects. Section 6 summarises the correlation trends to establish some of
77 the key causes of damage. This section also highlights the limitations of the indices and presents a brief discussion on how they
78 can be improved.

79 **2. Building damage survey**

80 In the two field studies performed by the authors between 13.03.23-20.03.23 and 11.04.23-21.04.23, 29 stone masonry
81 buildings consisting of 10 churches, 8 mosques, 6 public and 5 residential buildings were investigated. All the examined buildings
82 were constructed using unreinforced masonry and did not include metal reinforcements or timber tie beams (except for one
83 building where sporadic timber tie beam use was noted but judged ineffective). The buildings were chosen as they represent
84 monumental examples of the unique architectural heritage of the region. The investigated structures are associated with an ID
85 and province in Table 1. The examined buildings are from the Mamluk, Ottoman, French Mandate and Early Turkish Republic
86 periods. Specific dates of construction are not reported due to uncertainties in the architectural and historical resources examined
87 by the authors. Due to frequent seismic events in the area, many of the examined buildings underwent periodic repair, retrofit
88 and reconstruction activities, the extent of which is unclear. The last major earthquakes in the region date to the second half of
89 the 19th century (Över et al., 2011); historical records suggest that existing buildings may have been subjected to substantial

90 repairs during the intervening period. The original timber floors of some buildings (M5, P1-P4) were replaced with reinforced
 91 concrete (RC) slabs during more recent works (see Table A1).

92 To evaluate the local seismic demand, each building is associated to the nearest strong-motion station with available data
 93 (AFAD, 2023). Only the records from the Pazarcık earthquake and Samandağ earthquake were considered since the Elbistan
 94 event was far away from the investigated structures (Fig.1a). Preliminary damage level classification of buildings is conducted
 95 using the five EMS-98 damage grades (DGs) which range from negligible damage to total collapse (Mavroulis et al., 2019). Fig.
 96 1b presents a graphical representation of damage classes and their description. To avoid ambiguity, EMS-98 classification was
 97 only conducted on the main walls of the structures. Non-structural walls (e.g. parapets), floor and roof systems (e.g. domes,
 98 vaults) and annexed structures (minarets, towers and porches) are not considered in the DG assignment. Figs.3a-e show the
 99 location of the investigated buildings in Iskenderun, Antakya, Samandağ, Altınözü (districts of Hatay) and Osmaniye. On the
 100 maps, building types are indicated with symbols and coloured according to the building DGs. General photographs of the
 101 buildings are presented alongside detailed damage photographs.

102 Table 1. ID, name, type and province of investigated historic masonry buildings associated with the nearest strong-motion
 103 stations

ID	Building Name	Type	Province	Pazarcık earthquake		Samandağ earthquake	
				6 February 2023 ($M_w=7.8$)		20 February 2023 ($M_w=6.3$)	
				Station	Distance (km)	Station	Distance (km)
C1	Surp Karasun Manuk Church	Church	Hatay	3115	4.4	3119	1.4
C2	St. Nicholas Orthodox Church	Church	Hatay	3115	4.2	3119	1.3
C3	Latin Catholic Church	Church	Hatay	3115	4.5	3119	1.6
C4	Syriac Catholic Church	Church	Hatay	3115	4.4	3119	1.4
C5	Batayaz Armenian Church	Church	Hatay	3140	9.4	3140	9.4
C6	The Virgin Mary Samandağ Orthodox Church	Church	Hatay	3140	4.6	3140	4.6
C7	St. Ilyas Orthodox Church	Church	Hatay	3140	4.5	3140	4.5
C8	St George Sarılar Orthodox Church	Church	Hatay	3136	0.8	3136	0.8
C9	The Virgin Mary Tokaçlı Orthodox Church	Church	Hatay	3136	1.9	3136	1.9
C10	St George Iskenderun Orthodox Church	Church	Hatay	3115	3.5	3119	0.7
M1	Habib-i Neccar Mosque	Mosque	Hatay	3132	0.8	3124	3.8
M2	Sarımiye Mosque	Mosque	Hatay	3131	0.9	3124	4.0
M3	Şeyh Ali Mosque	Mosque	Hatay	3132	0.6	3124	3.7
M4	Kurşunlu Han Mosque	Mosque	Hatay	3132	0.9	3124	3.7
M5	Enverül Hamit Mosque	Mosque	Osmaniye	8003	2.1	8003	2.1
M6	Ağcabey Mosque	Mosque	Osmaniye	8002	2.4	2709	11.6
M7	Ala Mosque	Mosque	Osmaniye	8004	0.9	8004	0.9
M8	Hamidiye Mosque	Mosque	Osmaniye	8004	0.7	8004	0.7
P1	Hatay Metropolitan Municipality Building	Public	Hatay	3123	1.2	3124	3.8
P2	Mithatpaşa Primary School	Public	Hatay	3115	4.5	3119	1.6

P3	Yedi Ocak Primary School	Public	Osmaniye	8003	2.2	8003	2.2
P4	Antakya High School	Public	Hatay	3123	1.1	3124	3.9
P5	Iskenderun High School	Public	Hatay	3115	4.0	3119	1.1
P6	Olive Museum	Public	Hatay	3136	2.0	3136	2.0
R1	Gali Mansion-I	Residential	Hatay	3132	0.4	3124	3.6
R2	Gali Mansion-II	Residential	Hatay	3132	0.4	3124	3.6
R3	Hıdırbey Gastronomy House	Residential	Hatay	3140	5.3	3140	5.3
R4	Vakıflı No.2 House	Residential	Hatay	3140	4.2	3140	4.2
R5	Old English School	Residential	Hatay	3140	4.0	3140	4.0

104

105

106

107

108

109

110

111

112

113

114

115

116

117

118

119

120

121

122

EMS-98 DGs provide an indication of damage level. To discuss the types of damage encountered in the field, another classification may be useful. Borri et al. (2020) proposed a ‘hierarchy of mechanisms’ considering three response categories: i) masonry disaggregation, ii) local response, and iii) global response. Masonry disaggregation refers to the detachment of masonry units and mortar when subjected to strong ground motions. It is generally observed when weak mortar is used alongside irregular small stones (see Figs.2a-b). The second classification, local response, refers to the presence of mechanisms featuring one or more structural components. It generally involves out-of-plane motion. It is observed when masonry disaggregation is limited but effective wall to wall connections are not present to prevent the detachment of structural components. For instance, the overturning of the entire façade (e.g. C4 in Fig. 3a) or the first storey walls and the roof of a building in its transverse (e.g. short) direction (e.g. P2 in Fig. 3a) are classified as local response. The third classification, global response, is expected for structures with good construction quality and effective load transfer between masonry walls. Global response classification implies in-plane damage, such as flexural and shear cracking, concentrated around wall openings (e.g. P1 in Fig.3b, M5 in Fig.3e). The absence of visible structural damage in the walls was taken as global response (e.g. C1 in Fig. 3a, C5 in Fig. 3c). Further general information about the investigated buildings are presented in Appendix (see Table A1) for interested readers.

For the buildings examined, multiple response types had to be assigned as disaggregation was often observed alongside local or global response mechanisms. Fig.2a shows an instance where a local response mechanism involving the separation of building façades is seen alongside disaggregation. In Fig. 2b, the upper part of the disaggregated and leaning wall appears to have initiated a local response leading to vault collapse due to spreading supports. The EMS-98 DG and building response type are listed in Table 2.

123



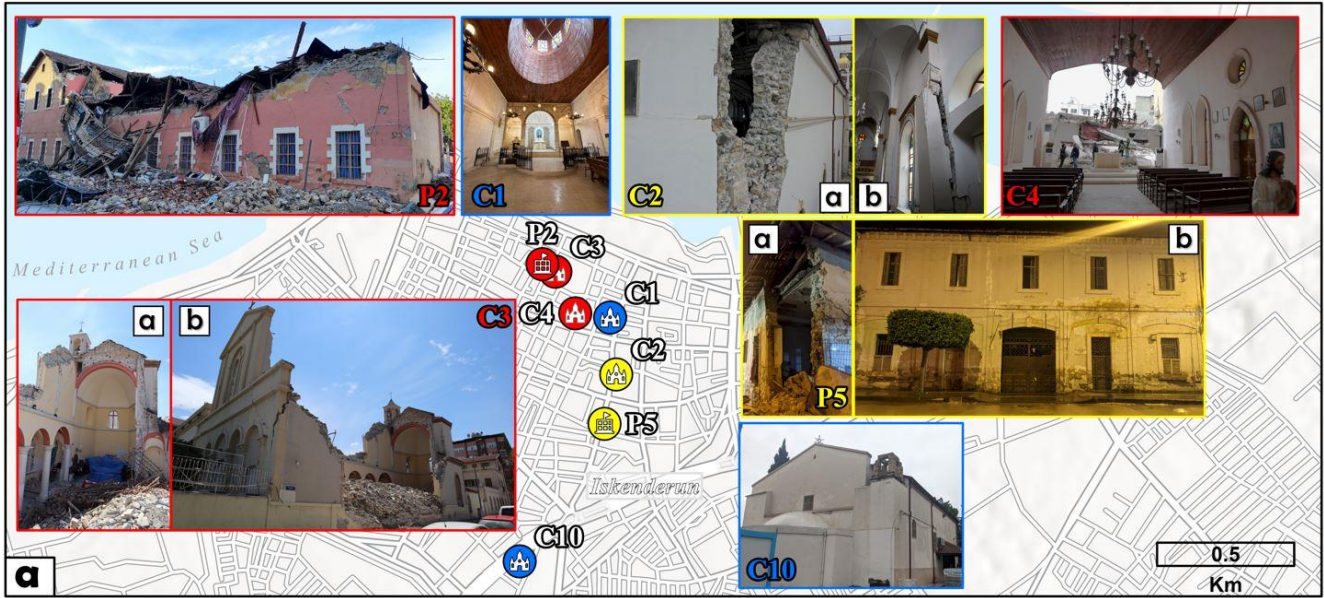
124

(a)

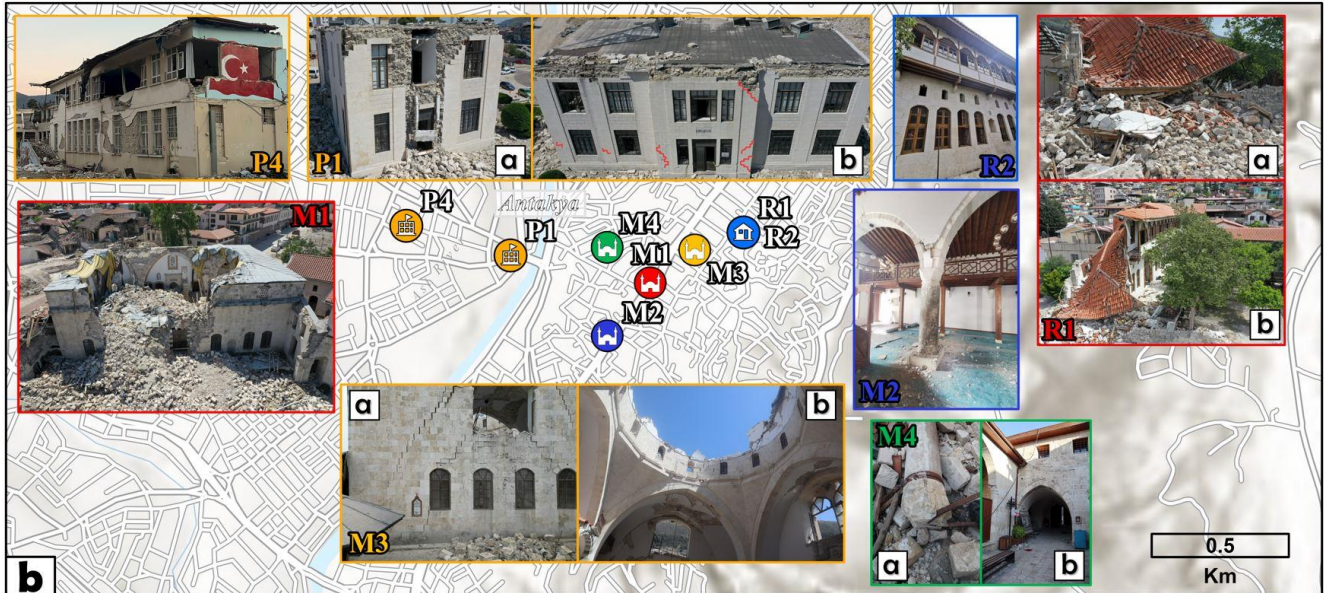
(b)

125

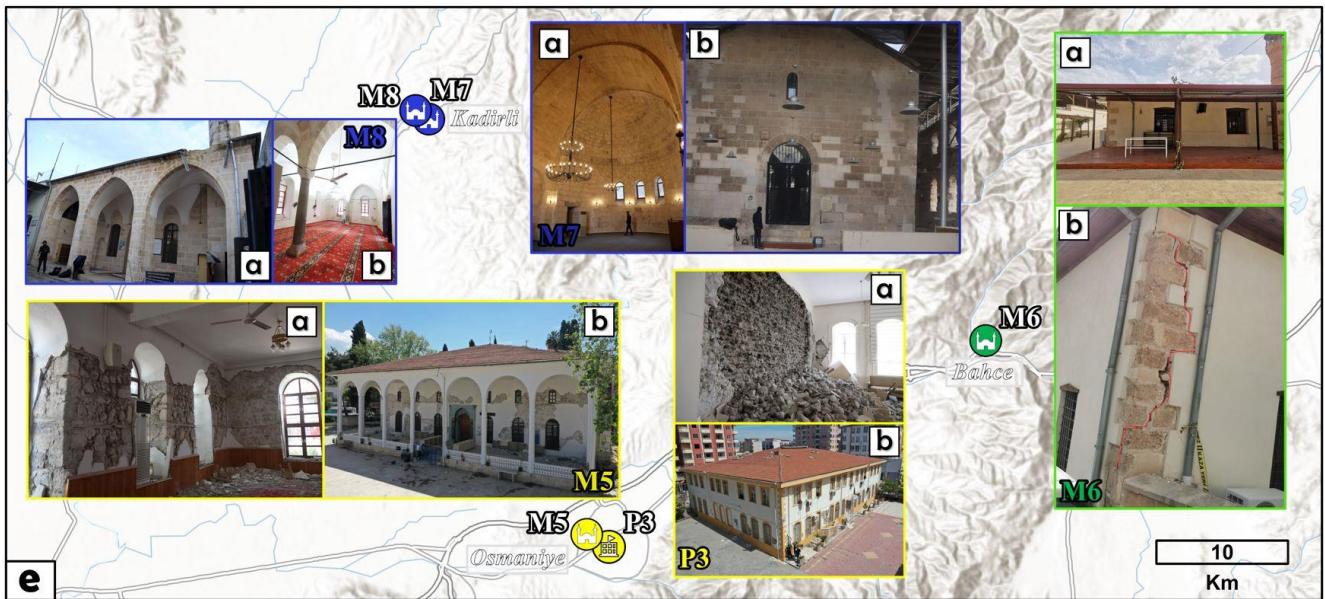
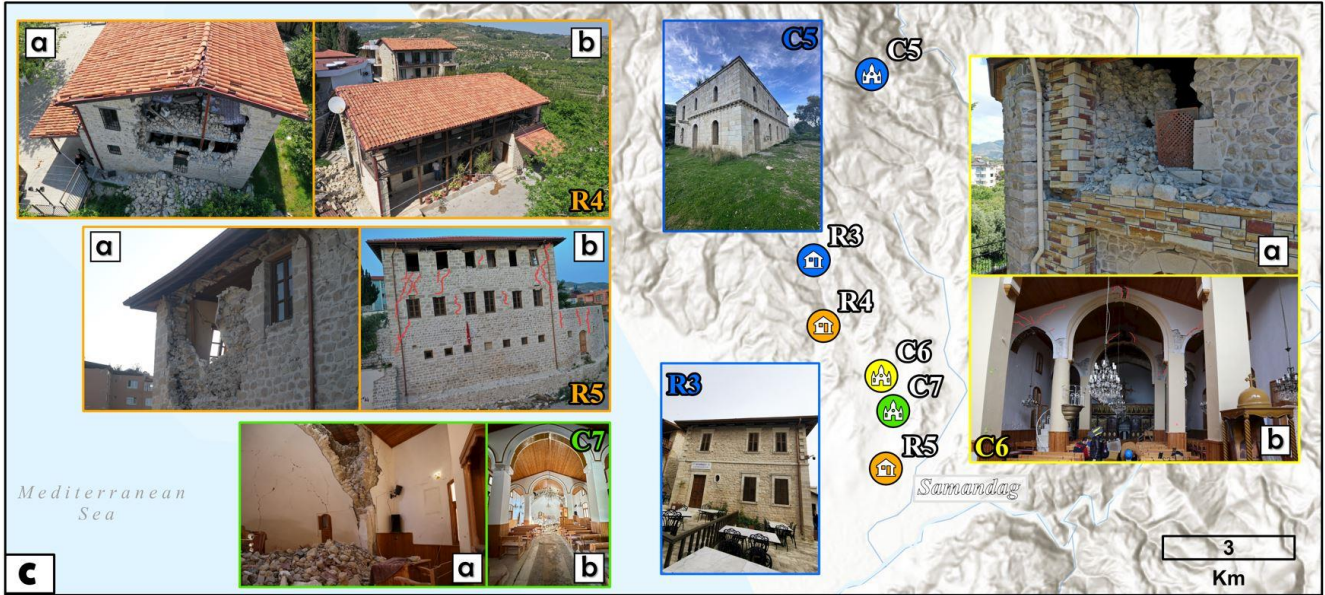
Fig.2 Partially disaggregated masonry walls and local response mechanisms from a) R1 and b) C8.



126



127



131 Fig.3. Location, EMS-98 DGs and photographs of the investigated buildings from a) İskenderun b) Antakya c) Samandağ d)
132 Altınözü e) Osmaniye

133 To aid damage evaluation, Table 2 also presents the resultant peak ground acceleration (PGA) values from the stations listed
134 in Table 1 for the 6 February and the 20 February earthquakes. The resultant PGA values are calculated by processing the N-S
135 and E-W acceleration records (Banerjee Basu and Shinozuka, 2011) to consider the maximum PGA value independent from
136 building main directions. Table 2 indicates that the largest PGA was 0.66g and recorded in the district of Antakya on the 6th of
137 February. This is consistent with the USGS surface fault rupture map in Fig. 1, which indicates that the district of Antakya lies
138 on the fault rupture footprint. Preliminary investigation reports (Taftsoglou et al., 2023; Ozturk et al., 2023) suggest that ground
139 motion within Antakya varied significantly due to local site conditions and basin effects; this is reflected in the range of PGA
140 values, 0.42-0.66g in Table 2, recorded in this district. Noteworthy vertical accelerations were also recorded in Antakya (Sagbas
141 et al., 2023) and may have had a significant influence on structural behaviour; however, this aspect remains outside the scope of
142 this first investigation. The resultant PGA magnitudes for the other districts are ordered from the largest to smallest as follows:
143 Altınözü, İskenderun, Bahçe, Samandağ, Kadirli and Merkez. The Samandağ earthquake was located close to the districts of
144 Antakya, Altınözü and Samandağ (listed in decreasing order of resultant PGAs) and caused resultant peak accelerations
145 exceeding 0.2g. Partial collapses of several buildings in these districts (e.g. C7 and R4 in Fig.3c) reportedly occurred during the
146 Samandağ earthquake. However, since the damage assessments were conducted after the Samandağ earthquake (20 February),
147 progressive evaluation of damage is not possible. In the following, the larger of the resultant PGAs from the Pazarcık and
148 Samandağ earthquakes will be considered as representative of the seismic demand.

149 Evaluating spectral accelerations of the buildings require knowledge of natural vibration periods. Simplified natural period
150 estimations for masonry buildings can be found in the literature. Several national design codes (ASCE/07-16, 2017; NCSE-2002,
151 2002; NTC-2008, 2008) suggest empirical formulae with respect to one (e.g. total height of the building) or two (e.g. total height
152 of the building and length of the building in plan) variables. However, these simplified approaches are only suitable for regular
153 building type structures with a uniform mass distribution along their heights. The accuracy of one or two variable natural period
154 estimation formulas is found to be low for special masonry structures; previous studies noted the need for more refined
155 formulations for special structures as churches (Lopez et al., 2019) and mosques (Çalik et al., 2020). The simplified period
156 estimation approaches are not adopted in this paper considering the large variation of key aspects (e.g. material, wall morphology,
157 opening, foundation and soil properties) amongst the investigated structures. Regardless, the acceleration spectra for each station
158 listed in Table 1 are presented in the Appendix (see Figs.A1a-e and Figs.A2a-e) for reference.

159
160
161

Table 2. Seismic response type (Borri et al., 2020) and damage classification of buildings with resultant PGA values

Building (wall construction)	District	Resultant PGA (g)		Response type			DG (EMS-98)
		6 February 2023 ($M_w=7.8$)	20 February 2023 ($M_w=6.3$)	Disaggregation	Local	Global	
C1 (RSM)	İskenderun	0.33	0.12			X	DG1
C2 (ISM)	İskenderun	0.33	0.12	X	X		DG3
C3 (RSM)	İskenderun	0.33	0.12	X	X		DG5
C4 (ISM)	İskenderun	0.33	0.12		X		DG5
C5 (RSM)	Samandağ	0.26	0.22			X	DG1
C6 (ISM)	Samandağ	0.26	0.22	X	X		DG3
C7 (ISM)	Samandağ	0.26	0.22	X	X		DG2
C8 (ISM)	Altınözü	0.54	0.33	X	X		DG4
C9 (ISM)	Altınözü	0.54	0.33	X	X		DG5
C10 (n/a)	İskenderun	0.33	0.12			X	DG1
M1 (RSM)	Antakya	0.58	0.54	X	X		DG5
M2 (RSM)	Antakya	0.42	0.54			X	DG1
M3 (RSM)	Antakya	0.58	0.54	X	X		DG4
M4 (RSM)	Antakya	0.58	0.54	X		X	DG2
M5 (ISM)	Merkez	0.19	0.04	X		X	DG3
M6 (RSM)	Bahçe	0.29	0.02		X		DG2
M7 (RSM)	Kadirli	0.20	0.01			X	DG1
M8 (RSM)	Kadirli	0.20	0.01			X	DG1
P1 (RSM)	Antakya	0.66	0.54	X		X	DG3
P2 (ISM)	İskenderun	0.33	0.12	X	X		DG5
P3 (ISM)	Merkez	0.19	0.04	X		X	DG3
P4 (RSM)	Antakya	0.66	0.54	X		X	DG4
P5 (ISM)	İskenderun	0.33	0.12	X		X	DG3
P6 (RSM)	Altınözü	0.54	0.33	X	X		DG4
R1 (RSM)	Antakya	0.58	0.54	X	X		DG5
R2 (RSM)	Antakya	0.58	0.54	X		X	DG1
R3 (RSM)	Samandağ	0.26	0.22		X		DG1
R4 (RSM)	Samandağ	0.26	0.22	X	X		DG4
R5 (RSM)	Samandağ	0.26	0.22	X		X	DG4
Incidence of response type (%)				~70	~50	~50	

163 The first column of Table 2 broadly specifies the wall construction technique (i.e. whether the external wall is faced with
164 Regular Stone Masonry (RSM) or Irregular Stone Masonry (ISM)), while the last row summarises the incidence of response
165 type. Masonry disaggregation was observed in 70% of the investigated buildings and in almost all of the ISM walls. Half of the
166 buildings featured crack patterns indicative of the formation of local mechanisms (50%) – most of these also experienced some
167 level of disaggregation. Global response with box-like behaviour was observed in 50% of the investigated buildings; these
168 buildings either featured in-plane flexural and shear cracks or no visible damage. Floor structures in some of these buildings
169 (M5, P1 and P3) were either reconstructed or retrofitted with reinforced concrete slabs, which ensured diaphragm action and
170 confined the response to in-plane mechanisms. Some buildings with timber floor structures (e.g. R2 and R5) also experienced

171 global response. Correlations between the damage level or response type with the building type (e.g. church) can also be explored
172 from Table 2. However, significantly different architectural designs (see Figs.3a-e), a wide range of material properties (see
173 Tables 6-7) and wall morphologies (see Fig.5) are observed for each building type. Therefore, the authors do not explore
174 correlations between response and damage level and type in the paper.

175 The damage survey presented in this section indicates that masonry disaggregation was commonly observed, often alongside
176 the formation of local response mechanisms. To better understand the potential reasons for these dominant mechanisms, the next
177 section explores wall geometry indexes.

178 3. Wall geometry assessment

179 The wall geometry indices or simplified seismic indexes (Lourenço et al., 2013; Lourenço and Roque, 2006) were established
180 to screen the damage vulnerability of monumental masonry buildings. These indices use wall geometry and local PGA
181 information to judge if a structure is 'safe' or 'unsafe'. They were formulated for large span monumental masonry structures and
182 their performance was evaluated using data from damage to monumental buildings in Europe and New Zealand. In this paper,
183 geometry indices are used as a diagnostic tool to establish the potential role of geometric aspects on damage.

184 There are two sets of indices: in-plane and out-of-plane. In-plane indices are useful to understand whether the building has
185 enough walls to carry the horizontal seismic loads in-plane in each direction. If the amount of walls are insufficient, local
186 mechanisms involving out-of-plane motion of structural components may be initiated. Out-of-plane indices evaluate the stability
187 of walls against overturning failure. Thresholds define safe-unsafe boundaries; the safe classification indicates buildings which
188 are safe to enter after an earthquake. This should correspond to DG3 or lower damage levels.

189 The first in-plane index is the ratio of the plan area of walls in one main direction of the building to the total plan area of the
190 building. For the design of new buildings, Eurocode 8 suggests a minimum safe value of 5-6% for regular masonry structures
191 for ground accelerations not exceeding 0.2g. In the literature, a safe value of 10% is recommended for historic masonry buildings
192 located in high seismicity regions (Meli, 1994). Lourenço et al.'s (2013) suggestion to adopt a safety threshold of 10% for PGA's
193 up to 0.25g and a linear increase for higher PGA's is followed in this study. Eqs. (1) are used to calculate the first in-plane index
194 for the transverse (x) and longitudinal (y) directions:

$$195 \lambda_{11x} = \frac{A_{wx}}{A_{plan}}, \lambda_{11y} = \frac{A_{wy}}{A_{plan}} \quad (1)$$

196 where λ_{11} is the first in-plane index, A_w refers to the plan area of earthquake resistant walls (in either x or y direction, as indicated
197 in the subscript), and A_{plan} is the total plan area of the building.

198 The second in-plane index is the base shear ratio. It is the ratio of shear resistance of the building to the shear demand in each
199 main direction. Assuming zero cohesion and self-weight, the base shear ratio can be calculated using Eq.(2) (Lourenço et al.,

200 2013). Due to the rectangular plan geometry of the investigated buildings, A_{wy} is typically high when compared to A_{wx} . Therefore
 201 the second in-plane index will be calculated only for the x direction:

$$202 \quad \lambda_{i2} = \frac{\mu A_{wx}}{(A_{wx} + A_{wy}) \beta} \quad (2)$$

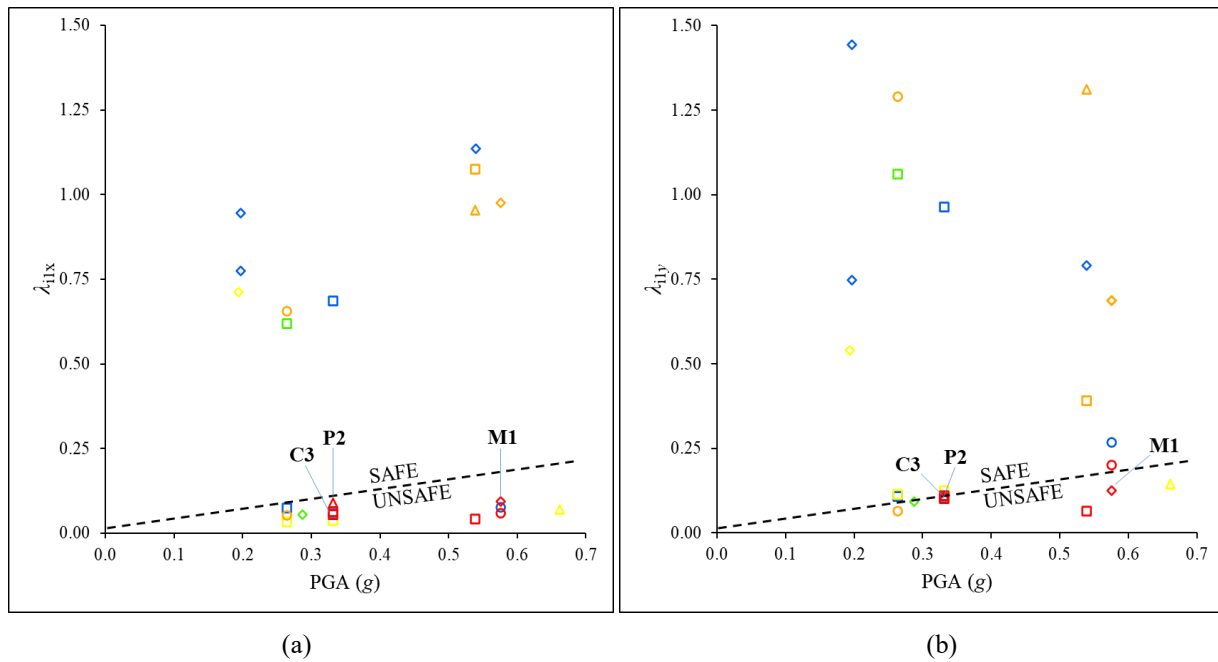
203 where λ_{i2} is the second in-plane index, μ is the coefficient of friction (assumed as 0.4 according to Eurocode 6 (2005)) and β is
 204 an equivalent seismic static coefficient (taken conservatively as the higher of the resultant PGA's from the Pazarcık and
 205 Samandağ event in Table 2). λ_{i2} values smaller than 1 indicate unsafe conditions where the demand is higher than the resistance.

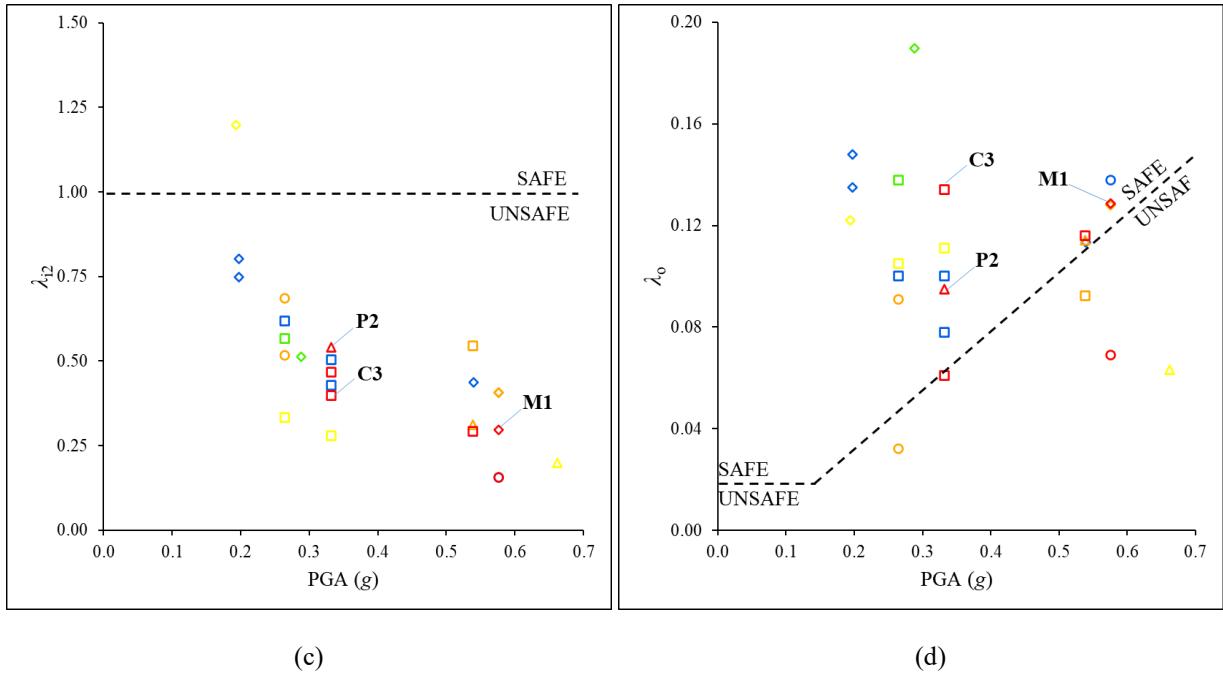
206 The geometric ratio of thickness to height of masonry walls is used as the out-of-plane index λ_o (Lourenço et al., 2013):

$$207 \quad \lambda_o = \frac{t_w}{h_w} \quad (3)$$

208 where t_w is the wall thickness and h_w is the average height of wall. Minimum values of λ_o are considered if there are different
 209 geometric configurations for walls in the same building. The slenderness ratio in Eq.(3) corresponds to the pseudo-static load
 210 capacity of an unanchored rigid rectangular block (Housner, 1963); if evaluated conservatively, it may indicate the PGA required
 211 to overturn the wall. However, Lourenço et al. (2013) suggested less conservative thresholds for the out-of-plane indexes using
 212 empirical observations. These are adopted in the current study.

213
 214





215

216

217

218

219

220

221

222

223

224

225

226

227

228

229

230

231

232

233

234

235

236

Fig.4. Relationship between a) λ_{i1x} and PGA b) λ_{i1y} and PGA c) λ_{i2} and PGA d) λ_o and PGA (\square : church, \diamond : mosque, Δ :public, \circ : residential, blue: DG1, green: DG2, yellow: DG3, orange: DG4, red: DG5 according to EMS-98)

Drawings of only some of the examined structures were available and were used to determine the geometric parameters required to calculate the indices. For structures without drawings, laser scanning and photogrammetry data collected during the post-earthquake field work were processed to extract the required parameters. Figs.4a-b show the relationship between λ_{i1} in x and y directions and PGA. In these figures, markers indicate the data from individual buildings, where the marker type indicates building category (e.g. square markers refer to churches). The markers are colour coded with reference to their DGs. According to Figs.4a-b, ~42% of the buildings are unsafe according to λ_{i1x} in the transverse direction, ~38% of the buildings are unsafe according λ_{i1y} in the longitudinal direction. The differences between these index results from the two directions are due to the typically larger plan area of walls in the longitudinal direction of buildings.

The results for the second in-plane index in the transverse direction in Fig.4c indicate that only one building is in the safe region. All buildings with DG levels 1 and 2 are located in unsafe areas. This indicates that in its current form, the second in-plane index in-plane provides a conservative assessment of safety. This is to be expected since important factors such as the contribution of material resistance (due to cohesion and tensile capacity) and other load distribution systems (such as rigid diaphragms, see concrete floors in P1 Fig.3b, or transverse arched frames in church naves, see C6 in Fig.3c) are neglected in the index calculations. However, the large percentage of unsafe classifications in the in-plane indices highlight a potential deficit for the examined structures in terms of their wall area to resist the earthquakes. The fact that all collapsed structures (DG5) are located in the unsafe regions of Figs.4a-c corroborates this statement.

As mentioned earlier, insufficient in-plane resistance in the transverse direction may lead to the formation of local mechanisms involving out-of-plane motion of structural components. The collapse of the structures rated DG5 in Table 2

237 (including C3, M1 and P2) was due to local mechanism formation and out-of-plane motion of walls in the building transverse
238 direction (see Fig. 3). To evaluate the vulnerability of walls to overturning instability during out-of-plane motion, Fig.4d explores
239 the relationship between λ_o and PGA. According to Fig.4d, only 5 of the buildings have unsafe walls, indicating that the walls of
240 structures were, in general, sufficiently thick to prevent out-of-plane instability. However, several building walls in the safe zone
241 of Fig.4d (including C3, M1 and P2) collapsed in the out-of-plane direction. While the indices of only a small number of buildings
242 are discussed in the text for brevity, the numerical values of seismic indices for each building can be found in the Appendix (see
243 Table A2).

244 Overall, the in-plane indices indicate insufficient amount of walls, especially in the building transverse direction. This deficit
245 may partially explain the formation of local mechanisms for many of the examined structures. The out-of-plane index suggests
246 that walls were sufficiently thick to prevent overturning instabilities. This contradicts the damage survey observations in Section
247 2, where multiple collapse cases due to out-of-plane action were noted. This apparent contradiction is related to the poor
248 construction quality of walls, which led to disaggregation and significantly reduced their out of plane capacity. This aspect is
249 investigated next.

250 4. Construction quality evaluation

251 Masonry disaggregation under horizontal seismic actions is one of the main reasons for out-of-plane damage in thick masonry
252 walls. Stone masonry constructions are typically composed of multiple leaves and the quality of connection between them
253 significantly affects their seismic response behaviour. The absence of good inter-leaf connections and weak adhesion between
254 stone and mortar may make historic stone masonry walls vulnerable to disaggregation (Maccarini et al., 2018). A qualitative
255 index called Masonry Quality Index (MQI) was proposed in (Borri et al., 2015) to account for the quality of masonry
256 constructions in historic masonry buildings. Borri et al. (2020) relate the index values to the expected masonry failure modes.
257 For instance, poor quality masonry walls with a low MQI are considered prone to disaggregation as a result of out-of-plane
258 actions. To understand if poor masonry construction quality is the cause of disaggregation for the structures in Table 2, this
259 section investigates their MQI.

260 To calculate MQI, the conservation state (SM), stone dimensions (SD), stone shapes (SS), wall-leaf connections (WC), mortar
261 joint geometry (HJ and VJ), and mortar quality (MM) parameters are evaluated. For each parameter, one of the following grades
262 is given: F (fulfilled), PF (partially fulfilled) and NF (not fulfilled). MQI is then calculated using a simple formula which weighs
263 parameters according to their importance for the given loading scenario. In this paper, only MQI of walls under horizontal out-
264 of-plane actions is calculated:

$$265 \quad MQI = SM (SD + SS + WC + HJ + VJ + MM) \quad (4)$$

266 where MQI represents the masonry quality index value for horizontal out-of-plane action. The numerical values of the parameters
267 required to calculate MQI under a given action, for a chosen fulfilment level (NF, PF or F) are provided in Table 3 and the

268 fulfilment criteria are discussed next. It should be noted that the MQI calculations may not be limited to out-of-plane actions; it
 269 is possible to calculate MQI indices for in-plane and vertical loads. However, as discussed earlier in Section 2, damage observed
 270 in the investigated buildings is primarily due to the weak out-of-plane resistance of the walls (e.g. insufficient wall-leaf
 271 connections). Therefore, for brevity, only the out-of-plane MQI index (*MQI*) is considered in this study.

272 Table 3. Numerical values of the parameters (*SM*, *SD*, *SS*, *WC*, *HJ*, *VJ* and *MM*) used to calculate MQI under horizontal out-of-
 273 plane actions for various fulfilment levels (NF, PF and F) (Borri et al., 2020)

Parameter	<i>MQI</i>		
	NF	PF	F
<i>SM</i>	0.5	0.7	1
<i>SD</i>	0	0.5	1
<i>SS</i>	0	1	2
<i>WC</i>	0	1.5	3
<i>HJ</i>	0	1	2
<i>VJ</i>	0	0.5	1
<i>MM</i>	0	0.5	1

274
275



276
277

Fig.5. Representative zoom-in views of typical walls investigated in Table 4

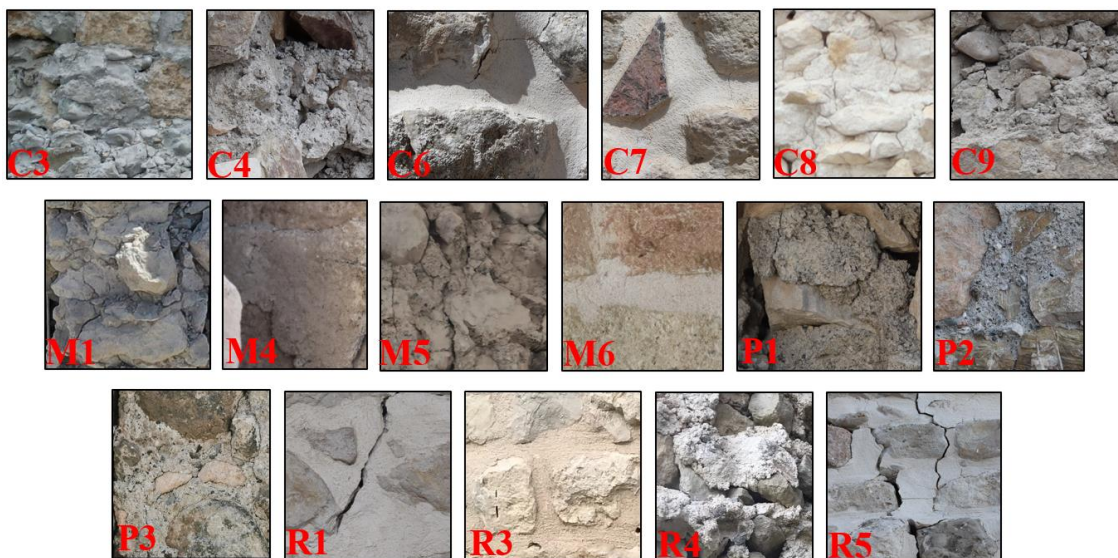


Fig.6. Representative zoom-in views of mortars investigated in Table 7

The fulfilment criteria for most MQI parameters are evaluated visually. For instance, the parameter *SS* refers to the shape of stonework. Representative cross-sections of walls and general view of mortars are shown in Figs.5-6, respectively. These indicate a wide variety of materials and construction techniques. ISM walls do not satisfy the fulfilment criteria for *SS* and are graded NF. RSM walls may be composed of cut stones through their thickness or may have distinct leaves. In Multi-Leaf Masonry (MLM) walls, the building external façade is often faced with cut-stones. If there is only one masonry leaf with cut-stone, the grade PF is given. If both external leaves are made of cut-stone, the grade F is given. Separately, the quality of mortar parameter *MM* is also evaluated visually, however, this evaluation is more subjective. It aims to classify the conservation state, strength, and regularity of mortar with a single parameter. In this classification, mortar in ISM walls is rated NF or PF. In MLM walls mortar is rated PF or F. In both cases, if the mortar is crumbly, the lower fulfilment level is chosen.

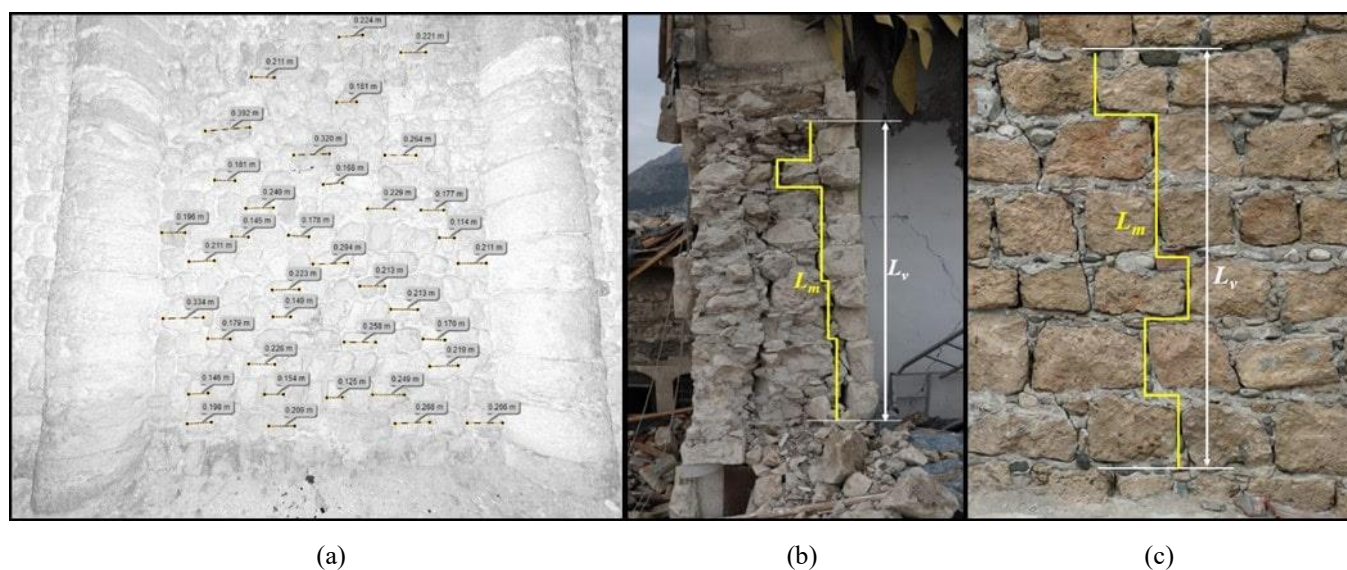


Fig.7. a) Stone dimension measurements from a point cloud (Building: C5), b) photograph of a through thickness cross-section of a disaggregated wall used for *WC* calculation (Building: M1), and c) an exposed wall surface used for *VJ* calculation (Building: C3)

294 Geometric measurements may be conducted to evaluate fulfilment criteria for some of the MQI parameters. For instance, the
 295 parameter SD refers to stone dimensions in the wall. The fulfilment criterion for this parameter is the presence of more than 50%
 296 of stones with length greater than 40 cm. SD can be calculated using individual stone size measurements from laser scan or
 297 photogrammetry point clouds (see Fig.7a). Another parameter that can be calculated qualitatively from point clouds or
 298 orthoimages is WC ; this calculation requires exposed through-thickness wall cross-sections. First, the distance between two
 299 points in vertical direction is measured (see L_v in Fig.7b). Then, for the same points, the length of the shortest connection path
 300 through mortar joints (see L_m in Fig.7b) is measured. WC fulfilment category is determined using the ratio of L_m to L_v (e.g. the
 301 criteria is F if $L_m/L_v > 1.6$). Another quantitative measurement option is available for the parameter of VJ , which can be evaluated
 302 from exposed masonry surfaces on the façade (see Fig.7c). The fulfilment category for VJ is F if $L_m/L_v > 1.6$. In this paper, the
 303 quantitative approaches were adopted whenever data was available. Otherwise, the qualitative approach was used following
 304 (Borri et al., 2015; Borri et al., 2020).

305 Once all the parameters are determined, Eq.(4) is used to calculate the MQI . The final value of MQI is used to assign the wall
 306 a quality category (A , B and C): $0 \leq MQI \leq 4$ is Category “C”, poor quality, $4 \leq MQI \leq 7$ is Category “B”, average quality, and 7
 307 $\leq MQI \leq 10$ is Category “A”, good quality. According to Borri et al. (2020), all Category “C” walls are prone to disaggregation.

308 Table 4 specifies the wall constructions broadly as ISM or RSM and presents the MQI classifications of 20 buildings where
 309 exposed masonry surfaces and/or through thickness cross-sections were available to enable the aforementioned parametric
 310 evaluations. The presence of disaggregation (obtained from Table 2) and the safety classification of the walls from the out-of-
 311 plane index λ_o (obtained from Fig. 4d) are also indicated in Table 4. All buildings constructed with ISM are in category “C”.
 312 This implies that masonry disaggregation is expected for this type of wall construction under horizontal seismic action.
 313 According to Table 4, all Category “C” buildings except C4 experienced masonry disaggregation. Some Category “B” buildings
 314 (M1, M3 and R1) also experienced masonry disaggregation. It should be noted that the wall internal connection criteria WC is
 315 not fulfilled (“NF”) for these buildings.

316 Table 4. MQI values and categories of buildings according to horizontal out-of-plane loading condition with λ_o and
 317 disaggregation evaluation

Building	Wall construction	MQI	Category	Out-of-plane seismic index (λ_o) safety criteria	Disaggregation
C2	ISM	1	C	Safe	Yes
C3	RSM	2.8	C	Safe	Yes
C4	ISM	1.4	C	Unsafe	No
C5	RSM	6	B	Safe	No
C6	ISM	0.35	C	Safe	Yes
C7	ISM	0.5	C	Safe	Yes
C8	ISM	1.4	C	Unsafe	Yes
C9	ISM	1.05	C	Safe	Yes
M1	RSM	6.5	B	Safe	Yes
M3	RSM	5.5	B	Safe	Yes

M5	ISM	1	<i>C</i>	Safe	Yes
P1	RSM	0.35	<i>C</i>	Unsafe	Yes
P2	ISM	0.7	<i>C</i>	Safe	Yes
P3	ISM	1	<i>C</i>	n/a	Yes
P5	ISM	0.7	<i>C</i>	n/a	Yes
P6	RSM	2.1	<i>C</i>	Safe	Yes
R1	RSM	5.5	<i>B</i>	Unsafe	Yes
R3	RSM	6	<i>B</i>	n/a	No
R4	RSM	2.8	<i>C</i>	Safe	Yes
R5	RSM	1.75	<i>C</i>	Unsafe	Yes

318

319 The data in Table 4 is useful to explain contradictory observations from Section 3. There, it was observed that several
320 collapsed buildings (e.g. M1, P2 and C3) were located in the safe zone of the out-of-plane seismic index λ_o . In other words, the
321 out-of-plane seismic index λ_o indicated that the total thickness to height ratio in these buildings should have been sufficient to
322 resist overturning instability. However, the MQI category of these buildings are either “*C*” or “*B*” and the wall internal connection
323 criteria *WC* are not fulfilled (“NF”). These results indicate that leaves may have separated during the earthquakes, reducing the
324 effective thickness of the wall in Eq.(3), and rendering it unsafe against overturning. For M1, separation of internal and external
325 leaves can be observed in Fig.7b. This disaggregation may have been responsible for the subsequent collapse of the mosque
326 dome (see Fig.3b). There are 11 buildings in Table 4, where the λ_o safety criteria is “Safe” but disaggregation is observed.

327 Despite the good correlation between masonry disaggregation observations and the MQI category “*C*”, it is important to note
328 that MQI cannot be used as a predictor of damage. MQI uses empirically defined weights to combine various quality measures
329 into a single scalar. However, as observed for M1, a specific weakness (e.g. as indicated the parameter *WC*) can lead to premature
330 failure in walls even though all other aspects of the construction are good. This is mentioned as a limitation of the MQI approach
331 in a recent review study, which also cites alternative construction quality indicators (Szabó et al., 2023). Furthermore, it is
332 important to note that the incidence of disaggregation damage relates to aspects that are not considered by the MQI, such as the
333 seismic demands on the wall and the supporting structural system. For example, the masonry quality in M5 is categorized as
334 “*C*”. However, disaggregation in this building remains limited due to comparatively low seismic demand and rigid diaphragm
335 action offered by the RC slab and frame system connecting masonry walls.

336 5. In-situ material measurements

337 Limited samples from only a small number of buildings could be collected for destructive testing in the laboratory due to the
338 heritage status of buildings. In the absence of laboratory samples, in-situ tests had to be conducted to quantify material properties
339 (see (Barnaure and Cincu, 2020) for a review of typical tests). Tests involving in-situ loading (e.g. flat jack test) could not be
340 applied due to safety concerns. Instead, the elastic modulus and compressive strength of stones were characterised using UPV
341 and SRH measurements, and the compressive strength of mortars were estimated using MP tests. The devices and procedures
342 used for the UPV, SRH and MP tests are discussed in the subsections 5.1.1, 5.1.2 and 5.1.3. The numerical data obtained for

343 material properties are presented in Section 5.2. Established correlations from the literature are also used in this section to derive
344 various other relevant material parameters (such as cohesion and friction angle of mortars) and the mechanical properties of
345 homogenised masonry walls.

346 5.1. Measurement techniques

347 All the in-situ measurements were performed on the walls of the investigated buildings. Intact loose stones from the building
348 debris were used for measurement when available. The SRH and UPV measurements were taken on all visually distinguishable
349 stone types. A minimum of two stones of each type were considered to evaluate variability and up to five stone types per building
350 were investigated. Surface and internal MP tests were performed at least from three different locations for at least two walls per
351 building.

352 5.1.1. UPV measurements

353 UPV test makes use of the fact that ultrasonic waves propagate at different velocities through materials with varying densities
354 and mechanical properties. By measuring the time it takes for waves to travel, wave propagation velocity can be determined.
355 This can then be used to estimate material properties such as density (ρ_s) (Gardner et al., 1974) and dynamic elastic modulus
356 (E_{dyn}) (Gonen and Soyoz, 2021). UPV tests are conducted using the following equipment: i) Transmitter: A transducer that
357 generates the ultrasonic waves sent into the sample, ii) Receiver: A transducer that measures the ultrasonic waves that travelled
358 through the stone, iii) Controller: A device for generating the electrical signals sent to the transmitter and digitising the signals
359 from the receiver. The controller also processes the signals (using the time and distance of travel) to obtain the P-wave velocity,
360 V_p .

361 When measuring stones in-situ, UPV tests were performed using indirect transmission (Fig.8a). The direct transmission
362 technique was used when measurements were conducted on loose stones (Fig.8b). PUNDIT PL-200 testing device with 54 Hz
363 exponential transducers were used. The exponential transducers were preferred as they can conduct measurements on rough
364 surfaces without coupling agents (Wróblewska et al., 2021). The UPV device was calibrated regularly (e.g. when the subject
365 wall or building changed) using the special calibration rod (see Fig.8b) to minimize measurement errors. The velocity
366 measurements were repeated three times and averaged to obtain V_p .



367 (a)



368 (b)

369 Fig.8. a) Indirect UPV measurement on an in-situ stone from R4, and b) direct UPV measurement on a disaggregated stone from
370 C3

371 The following equation can be used to estimate E_{dyn} (Marazzani et al., 2021):

$$372 \quad E_{dyn} = \frac{V_p^2 \rho_s (1 + \nu_s)(1 - 2\nu_s)}{(1 - \nu_s)10^6} \quad (\text{MPa}) \quad (5)$$

373 where ν_s is the Poisson's ratio for the stone. The units for V_p and ρ_s in Eq.(5) are m/s and kg/m³, respectively. It can be observed
374 from Eq.(5) that accurate estimation of E_{dyn} requires the use of appropriate ν_s and ρ_s values, in addition to measured wave velocity
375 V_p . In the literature, the value for Poisson's ratio of different stones varies between 0.13-0.33 (Li et al., 2023; Wang et al., 2024).
376 It will be assumed as 0.25 in this study. Since it was not possible to measure the density of in-situ stones, empirical relations
377 between ρ_s and V_p for natural stones were used (Gardner et al., 1974; Günaydin et al., 2022):

$$378 \quad \rho_s = 230V_p^{0.25} \quad (\text{kg/m}^3) \quad (6)$$

379 The accuracy of density estimation using Eq.(6) will be evaluated in Section 5.2.

380 The elastic modulus obtained using Eq.(5) is called "dynamic" due to the negligible strain levels during ultrasonic testing.
381 Static elastic modulus of stones (E_{sta}) is smaller compared to E_{dyn} . Several empirical equations were presented for different type
382 of stones to estimate E_{sta} using E_{dyn} (Eissa and Kazi, 1988; Al-Shayea, 2004; Brotons et al., 2014). In this study, Eq.(7) was
383 chosen to calculate E_{sta} as it was derived from a large dataset featuring different stone types (Eissa and Kazi, 1988; Gonen and
384 Soyoz, 2021):

$$385 \quad E_{sta} = 0.74E_{dyn} - 820 \quad (\text{MPa}) \quad (7)$$

386 The UPV tests were conducted in different parts of the building, on in-situ and loose stones. In MLM walls, measurements
387 were conducted on both ashlar and internal rubble stones. The results of these tests are averaged to estimate E_{sta} values for each
388 building.

389 5.1.2. SRH tests

390 The SRH is a portable instrument used for assessing the compressive strength of masonry stones. It measures the rebound of
391 a spring-loaded hammer after striking the surface of the material, providing an indirect estimation of its strength. A previous
392 study using cored sampled stated that the mechanical properties of samples from exterior surfaces are unlikely to be significantly
393 different from interior surfaces of the same stones (Ferreira Pinto et al., 2021). This indicates that if extensive surface degradation
394 is not present, surface hardness can be used to estimate the estimate compressive strength of stones.

395 In the field study, Silver SRH of Proceq was used. The Silver SRH uses optical sensors to measure the impact and rebound
396 velocity. These velocity measurements are used to calculate the Q value. As such, the Q value is not influenced by the friction
397 on the guide rod or the relative velocity between the unit and the specimen. It is also independent of the impact direction (Viles

398 et al., 2011). These aspects enable the use of Silver SRH for testing in-situ and loose stones. The Silver SRH is compatible with
399 a mushroom plunger that enables measuring compressive strengths as low as of 5 MPa (Kumavat et al., 2021).



400
401

402 Fig.9. a) Preparing phase of a stone for SRH test in building C2 b) SRH measurement on a stone from a collapsed wall of M1

403 Before applying the SRH, the surface of the stones is cleaned with polishing tool (Fig.9a). Fig.9b shows the SRH test being
404 performed on a loose stone sample. Ten readings were obtained by conducting rebound measurements in small area. Readings
405 are averaged to obtain the Q value that is used to calculate the compressive strength of stone (f_s):

406
$$f_s = 0.0108Q^2 + 0.2236Q \quad (\text{MPa}) \quad (8)$$

407 It should be noted that Eq.(8) is valid for Q values between 13 and 44 which corresponds to compressive strength values
408 between 5 and 31 MPa (Kocáb et al., 2019). The procedure was applied to in-situ and loose stones to estimate an average value
409 of f_s for each building.

410 5.1.3. MP tests

411 The mechanical properties of mortar may have a significant influence on the damage response of masonry walls. Since it is
412 unfeasible to extract large mortar samples from existing historic structures, it is often necessary to use non-destructive or minor
413 destructive techniques in-situ to evaluate mechanical properties of mortar. Penetrometer tests which evaluate the dynamic
414 penetration of a steel needle to estimate the compressive strength of mortar (Gambilongo et al., 2023; Žalský et al., 2023), is a
415 commonly used method. Another version of the penetrometer is based on a pin which is driven at constant velocity into the
416 mortar, where the applied load is obtained as a function of the penetration depth (Liberatore et al., 2016).

417 In this study, the MP device (see Figs.10a-b) of Diagnostic Research Company (DRC) was used to estimate the compressive
418 strength of mortars (f_m) from the investigated buildings. The MP device has a hammer that is attached to a manually loaded
419 spring. When released, the hammer strikes a steel needle and the mortar is exposed to dynamic blows with consistent impact
420 energy. This energy causes the needle's tip to penetrate the mortar. According to the manufacturer's instructions, the test should
421 be conducted by striking the needle 10 times. The penetration depth is then measured and used to calculate compressive strength
422 of mortar with Eq.(9):

423

$$f_m = \frac{5970 - \sqrt{(1.58d_m - 5.3)10^6}}{1580} \quad (\text{MPa}) \quad (9)$$

424

where d_m is penetration depth in mm. The equation is valid for penetrations in the range 4 to 22 mm (Gambilongo et al., 2023).

425

MP tests were performed both at the surface (Fig.10a-b) and internally, e.g. at an approximate depth of 8cm from the surface of the wall (Fig.10c). This was done to evaluate potential mechanical differences in mortar located in different parts of the wall.

427

The MP tests were performed multiple times in different parts of masonry walls on site and f_m values were calculated using

428

Eq.(9). Building-wide averages were then calculated for surface and internal measurements to obtain representative values for

429

each structure.



(a)



(b)



(c)

430

431

432

Fig.10. a) MP test for a thin mortar between corner cut-stones b) MP test for a thick mortar between irregular rubble stones

433

(building: C6) c) drilling of an access hole to perform an internal MP test on a thick mortar

434

5.2. Results and discussion

435

Correct estimation of E_{dyn} of stones relies on using the correct density value ρ_s in Eq.(5). Since it was not possible to measure

436

density of stones in-situ, the use of Eq.(6) to estimate ρ_s values were proposed. Before doing this, the accuracy of Eq.(6) was

437

evaluated by conducting gross density measurements on loose stones on site (e.g. by measuring their weight and roughly

438

estimating their volume). This verification was performed for several samples and the results are provided in Table 5. According

439

to the table, the maximum relative error for ρ_s is lower than 15%. This is considered acceptable since the loose stones on site

440

were not regular and consequently the ‘measured’ densities were approximate.

441

Table 5. Comparison of ρ_s values obtained from Eq.(6) and gross density measurements performed on loose stone samples

Stone sample	Building	ρ_s (kg/m ³)		% Difference
		Measured (by weighing on site)	Estimated (by Eq.(6))	
1	C6	1994.2	2287.7	14.7
2	C9	2144.8	2427.0	13.2
3	C9	2168.4	2404.4	10.9
4	M1	2411.7	2402.6	0.4
5	M2	2168.6	2144.2	1.1
6	M2	2033.0	2101.2	3.4

7	P1	2424.1	2231.5	7.9
8	P1	1826.9	1825.7	0.1
9	P1	2035.9	2266.4	11.3
10	P1	2109.7	2200.1	4.3
11	P1	2326.5	2299.2	1.2
12	R4	2281.6	2474.7	8.5
13	R4	2424.2	2332.4	3.8

442

443

444

445

446

447

448

449

450

451

452

453

454

When the UPV and SRH techniques are applied to the same stones, consistent results are obtained for the elastic modulus and compressive strength; these results show the expected correlations. However, such correlations depend on the type of stones. Since chemical characterisation of stones was not possible on site, this relationship is not explored further and individual results are not plotted here for brevity. Instead, building-wide averages for the static elastic modulus and compressive strength of stones are calculated. Table 6 shows that E_{sta} and f_s values vary between 2043-15261 MPa and 13.5-31.2 MPa, respectively. Although the estimated f_s values in Table 6 for some buildings (P1, R2 and R4) are slightly higher than the limit of Eq.(8), they are still reported for completeness. The standard deviation values for the compressive strength are also provided and indicate significant variability of strength estimates in both the RSM and ISM buildings. This is not surprising considering the wide variety of stones used in the walls. The average value of f_s is obtained as 25 and 26 MPa for buildings with ISM and RSM walls. The results further indicate that systematic differences are not observed between the average compressive strength values of ashlar and rubble stones used in MLM walls (not shown).

Table 6. Estimated static elastic modulus and compressive strength of stones of the investigated buildings

Building	Wall construction	E_{sta} (MPa)	f_s (MPa) average±standard deviation
C3	RSM	8726	13.5±5.2
C4	ISM	11538	18.5±8.9
C5	RSM	7956.4	24.1±3.4
C6	ISM	10553.8	26.2±4.3
C7	ISM	14461	23.5±6.5
C8	ISM	7645.6	25.2±3.5
C9	ISM	8578	26.1±6.2
M1	RSM	15260.2	26.9±4.5
M2	RSM	3398	22.2±8.6
M3	RSM	6506	26.5±2.1
M4	RSM	11604.6	28.5±2.6
M5	ISM	6128.6	25.9±6.5
M6	RSM	2043.8	28.2±1.8
M7	RSM	5114.8	27.4±3.2
P1	RSM	7690	28.6±3.5
P2	ISM	6787.2	24.7±5.4
P3	ISM	4471	21.8±5.5
R1	RSM	8859.2	28.6±1.8

R2	RSM	8755.6	31.2±2.7
R3	RSM	8407.8	28±5.9
R4	RSM	12041.2	31±3.9
R5	RSM	10442.8	21.7±7.5

455

456

457

458

459

460

461

462

463

464

465

Building-wide average mortar compressive strength values obtained from surface and internal MP tests are presented in Table 7. The values range from 0.4-2.2 MPa for surface tests and 0.6-3.1 MPa for internal tests. In general, compressive strength of mortars obtained from surface and internal tests indicate different values. Sometimes, due to repointing or more carbonation, mortars are stronger on the surface. At other times, mortars are stronger inside as they are exposed less to environmental weathering. In the absence of any clear trends, it is considered appropriate to consider the average of surface and internal values to represent mortar compressive strength. The average value of f_m is 1.48 MPa for RSM constructions while the corresponding value is 1.36 MPa for ISM which indicates there is no trend for mortar quality based on wall construction type. More generally, the data indicates that further investigations on historic buildings should consider weak mortar characteristics, with a typical capacity less than 2 MPa.

Table 7. MP test results with general view and type of the historic mortars

Building	Wall construction	Measurement		
		Surface	Internal	Average
f_m (MPa)				
C3	RSM	2.1	n/a	2.1
C4	ISM	1.2	n/a	1.2
C6	ISM	1.7	3.1	2.4
C7	ISM	2.2	0.7	1.45
C8	ISM	1.1	0.8	0.95
C9	ISM	2.2	1.8	2.0
M1	RSM	1.1	0.9	1.0
M4	RSM	1.5	2.9	2.2
M5	RSM	0.5	1.3	0.9
M6	RSM	1.5	1.2	1.35
P1	RSM	n/a	0.6	0.6
P2	ISM	0.5	n/a	0.5
P3	ISM	0.4	1.7	1.05
R1	RSM	1.3	1.0	1.15
R3	RSM	1.3	1.3	1.3
R4	RSM	2.0	2.0	2.0
R5	RSM	n/a	2.2	2.2

466

467

468

469

Average stone and mortar compressive strength values are plotted in Fig.11a. Other key parameters that may be used in numerical investigations include the cohesion (c) and the coefficient of friction of mortar (μ). c and μ were estimated using the average f_m values in Table 7 and interpolating the NZSEE recommendations (see Table 8) for non-cohesive, soft and firm historic

470 masonry mortar properties (Ghiassi et al., 2019). The resulting values are shown in Fig.11b, where the values of c and μ vary
 471 between 0.05-0.15 MPa and 0.2-0.5, respectively.

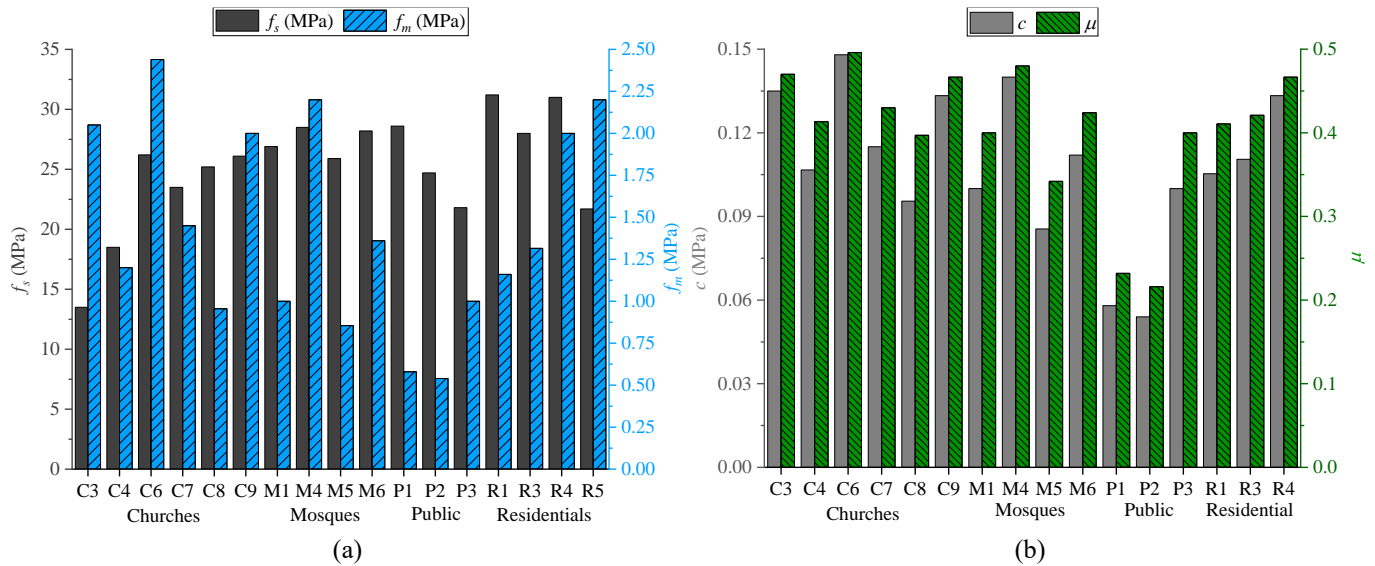
472 In Section 3, the seismic index λ_{i2} was calculated considering the suggested μ value of 0.4 for historic masonry buildings EC6
 473 (2005). Adopting the values estimated from material measurements and correlations to calculate the λ_{i2} seismic index, does not
 474 change the assignments for 'safe' or 'unsafe' designation of buildings in Fig. 4.

475 Table 8. NZSEE recommendations (NZSEE, 2006) for mechanical properties of mortar

Type	f_m (MPa)	c (MPa)	μ
Non cohesive	0	0	0
Soft	1	0.1	0.4
Firm	4	0.2	0.6
Stiff	8	0.4	0.8

476

477



478

479

480

Fig.11. a) Compressive strength values for stone and mortar b) tangent of friction angle and cohesion values

481 The compressive strength (f_{mas}) and elastic modulus (E_{mas}) of masonry walls are two key parameters required for the analysis
 482 homogenized masonry walls in finite element simulations. These parameters are estimated in various earthquake code of
 483 regulations using masonry constituents' strength properties. According to EC6 (2005) and TBEC (2018), the f_{mas} can be
 484 calculated as follows:

485

$$f_{mas} = \kappa f_s^\alpha f_m^\beta \quad (10)$$

486 where κ , α and β are considered as 0.45, 0.7 and 0.3 for masonry made with natural stone and general purpose/light weight
 487 mortar.

488

489 The modulus of elasticity of masonry walls can be estimated using Eq.(11) where ψ is a coefficient based on correlation
 490 between f_{mas} and E_{mas} and generally varies between 300 and 1000. The EC6 and TBEC (2018) consider ψ as 1000 and 750,
 respectively (Gonen and Soyoz, 2021).

$$E_{mas} = \psi f_{mas} \quad (11)$$

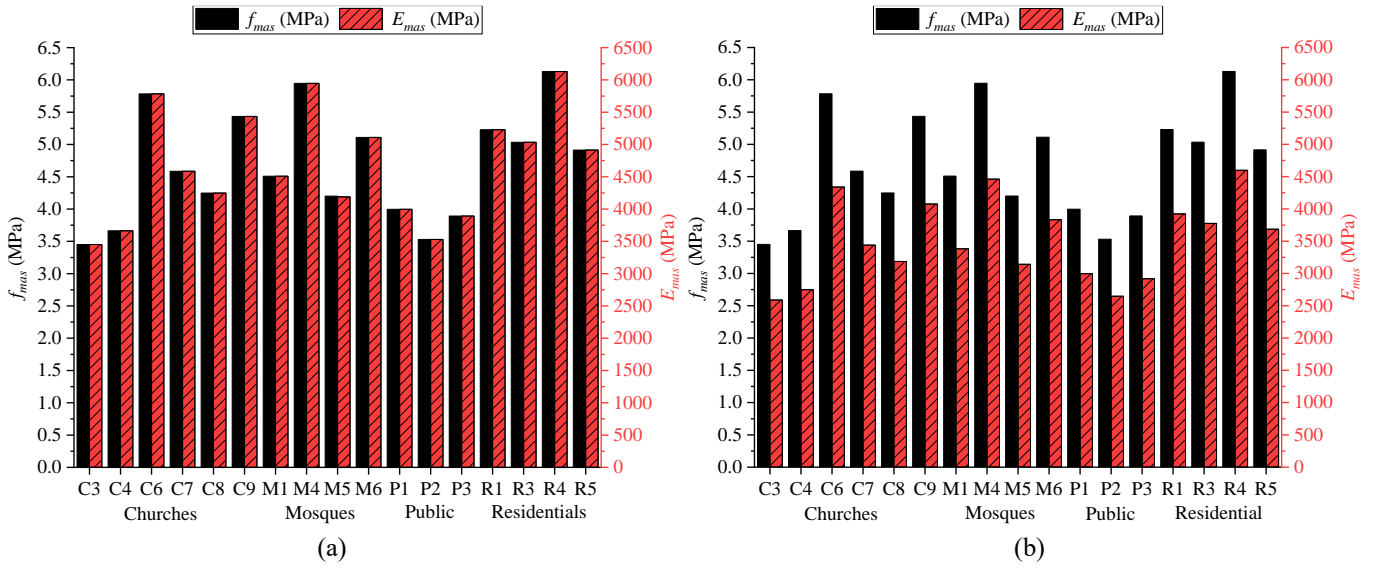


Fig.12. Compressive strength and elastic modulus values for masonry a) using EC6 equations b) using TBEC2018 equations

Using Eqs.(10-11), the f_{mas} and E_{mas} values are calculated. These are presented in Figs.12a-b for EC6 and TBEC (2018). f_{mas} ranges between 3.4 and 6.2 MPa according to EC6 and TBEC (2018), while E_{mas} varies between 3450-6130 MPa and 2585-4600 for EC6 and TBEC (2018), respectively.

6. Conclusions

To understand the damage experienced by the monumental stone masonry buildings in Hatay and Osmaniye provinces after the 2023 Turkey earthquakes, an assessment of wall geometry and construction quality was performed with state-of-the-art indices. The combined use of these indices provided new insight into response and may be explored not only as a post-earthquake but also as a pre-earthquake assessment tool in future studies. In addition, the mechanical properties of stones and mortars used in the building walls were estimated by in-situ non-destructive material tests. Conclusions from the investigations are summarised below:

- Inspection of in-plane wall geometry index (λ_{i2}), which is the ratio of base shear capacity to demand, indicates that most buildings did not have sufficient walls to resist the significant seismic demands that were experienced during the earthquakes. This deficiency may have promoted the out-of-plane failures observed in the collapsed buildings.
- The out-of-plane wall geometry index (λ_o) suggests that most building walls were sufficiently thick to resist the out-of-plane seismic failure. However, 70% of the investigated buildings experienced masonry disaggregation, which reduced the effective thickness of walls and led to out-of-plane collapse.
- According to MQI calculations, 75% of the investigated buildings are designated with class “C” which indicates poor masonry constructions prone to disaggregation under seismic actions. Majority of these buildings are constructed using

514 irregular stone masonry and experienced disaggregation. Some regular masonry constructions, including those with multi-
515 leaf walls, are characterised with weak inter-leaf connections, which explains their poor out-of-plane performance.

- 516 • In addition to poor connections, the widespread disaggregation failures indicate poor materials. In the scientific literature,
517 there was limited information on stone masonry materials used in the region. For this reason, Ultrasonic Pulse Velocity,
518 Schmidt Hammer and Mortar Penetrometer tests were conducted on site. The average compressive strength of stone and
519 mortar in buildings is estimated to range between 13.5-31.2 MPa and 0.5-2.4 MPa, respectively. This reflects the wide
520 variety of materials used in the region and indicates poor mortar quality which may have promoted disaggregation failures,
521 particularly in ISM walls. Using correlations from codes of guidance, the average compressive strength of masonry walls
522 was also estimated to vary between 3.4 and 6.2 MPa.

523 The data collected in this research also highlighted some limitations of the wall geometry and construction quality indices.

524 These are summarised below:

- 525 • The in-plane indices correctly estimated that collapsed buildings were ‘unsafe’. However, the second in-plane index
526 indications were excessively conservative and estimated that nearly all buildings (including undamaged ones) were
527 ‘unsafe’. To achieve more useful predictions with this index, it may be necessary to consider the influence of cohesion
528 and the weight of the building.
- 529 • In the presence of masonry disaggregation, the out-of-plane index thresholds provide unconservative assessments of
530 safety. Future evaluations should discard the use of this index in case of disaggregation.
- 531 • The MQI category “C” correlated well with masonry disaggregation. However, the occurrence of masonry
532 disaggregation depends on the local seismic demand; therefore, MQI should be seen as an indicator of disaggregation
533 vulnerability rather than a predictive index. Furthermore, correlations between damage patterns and MQI categories
534 indicated that specific parameters, such as wall-leaf connection, may have a dominant influence on wall behaviour.
535 Therefore, caution should be exercised in the use of MQI overall category as a potential indicator of wall load capacity.

536 Damage observations from the field also indicated that aspects which have not been considered in this study (such as floor
537 structures, progressive damage due to sequential earthquakes, soil-structure interaction and vertical ground accelerations) may
538 have influenced building damage. To understand the influence of these aspects, computational analyses are needed, which require
539 detailed knowledge of the mechanical properties of masonry constituents. It is hoped that the data presented in this paper will
540 form the basis of such further investigations.

541 **Acknowledgements**

542 The field work conducted as a part of this study was supported by EPSRC (via the grants EP/P025641/1 and EP/V048082/1)
543 and TUBITAK (2221-Fellowships for Visiting Scientists and Scientists on Sabbatical Leave Support Programme). Earthquake
544 Engineering Field Investigation Team (EEFIT) organised the first field mission. Baran Bozyigit acknowledges the financial

545 support of TUBITAK 2219-International Postdoctoral Research Fellowship Programme. The authors would like to thank Shirley
546 Underwood from Screening Eagle/Proceq for the loan of NDT equipment used in this research. Thanks are also due to DRC
547 Italia for supplying equipment at short notice. FARO UK provided free software licenses to enable laser scan data processing –
548 University of Oxford DPhil students Yilong Yang, Yixiong Jing and Zheng-You Zhang provided the processed data. The authors
549 are grateful to building owners and custodians for allowing them access; the list is too long to acknowledge here but special
550 thanks are due to Yusuf Tabasyan (İskenderun Karasun Manuk Church), Ratibe Bugrahan (Hatay Metropolitan Municipality),
551 Gokhan Cicek (Directorate of Foundations), Abdullah Papas (St George Sarilar Orthodox Church) and Dimyan Emektas (St
552 Ilyas Orthodox Church). Logistic help from Misel Uyar (Nehna) and Ahmet Cakmak (Istanbul Metropolitan Municipality) made
553 this work possible. We also acknowledge our academic collaborators, Prof. Heather Viles, Prof. Alper Ilki, Prof. Bora Pulatsu,
554 Prof. Eser Cakti, Prof. Paulo Lourenço and Dr Pascal Lava for contributing in various ways to this study.

555 Appendix

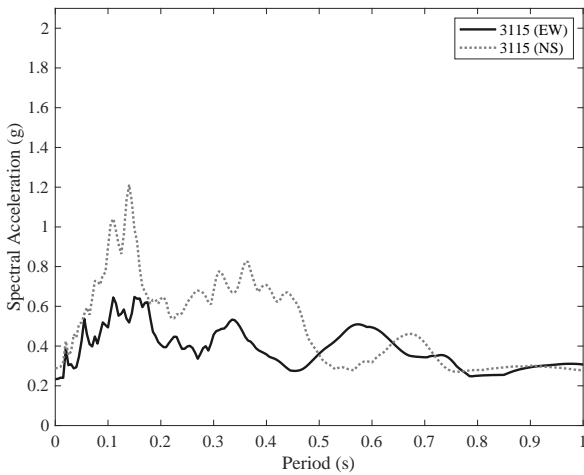
556 **Table A1. Additional geometric data and general information about the historical masonry buildings investigated**

ID	Wall properties			General information		
	Average height (m)	Typical thickness (m)	Typical number of leaves	Plan area (m ²)	Floor type	Roof type
C1	6.45	0.5	double-leaf	168	n.a.	Timber joist
C2	9	1	double-leaf	415	n.a.	Timber vault
C3	5.6	0.75	double-leaf	375	n.a.	Stone vault
C4	9	0.55	double-leaf	166	n.a.	Timber truss
C5	7	0.7	double-leaf	312	n.a.	Stone vault
C6	6.2	0.65	double-leaf	265	n.a.	Timber joist
C7	6	0.5	double-leaf	204	n.a.	Timber joist
C8	6.5	0.6	three-leaf	133	n.a.	Stone vault
C9	6.2	0.7	double-leaf	187	n.a.	Stone vault
C10	6.5	0.65	n.a.	234	n.a.	Timber joist
M1	8.5	1.1	three-leaf	374	n.a.	Stone dome and vaults
M2	4.85	0.55	n.a.	99	n.a.	Timber joist
M3	7.8	1	double-leaf	363	n.a.	Stone dome and vaults
M4	n.a.	n.a.	n.a.	n.a.	n.a.	Stone dome and vaults
M5	8.2	1	single-leaf	645	RC beam and slab	RC beams and slab
M6	4.6	0.9	single-leaf	551	n.a.	Timber truss
M7	7.4	1	double-leaf	640	n.a.	Stone vault
M8	6.75	1	n.a.	121.5	n.a.	Stone dome and vaults
P1	9.5	0.6	double-leaf	325	RC beam and slab	RC beams and slab
P2	4.2	0.4	double-leaf	200	Jack arch	Timber truss
P3	4.6	0.8	single-leaf	858	RC beam and slab	RC beams and slab
P4	n.a.	n.a.	double-leaf	n.a.	RC beam and slab	RC beams and slab
P5	n.a.	n.a.	double-leaf	n.a.	n.a.	Timber/steel joist
P6	5.25	0.6	double-leaf	88	n.a.	Stone vault
R1	4.35	0.3	double-leaf	82	n.a.	Timber joist
R2	4.35	0.6	single-leaf	70	Timber joist	Timber joist
R3	n.a.	n.a.	double-leaf	n.a.	Timber joist	Timber joist
R4	5.5	0.5	three-leaf	123.5	Timber joist	Timber joist
R5	11.5	0.4	double-leaf	150	Timber joist	Timber joist

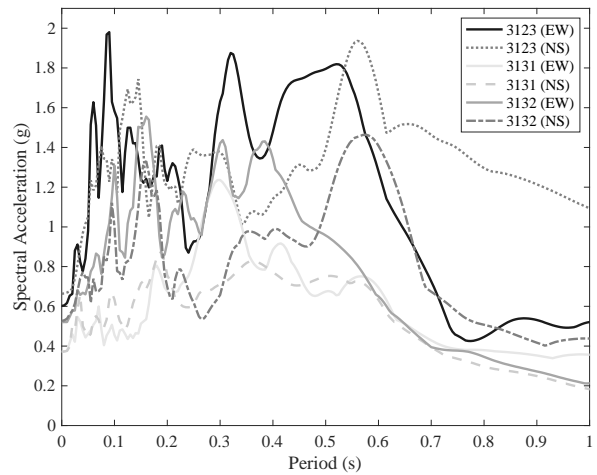
557

Table A2. The seismic indices of the investigated buildings according to wall geometry assessments

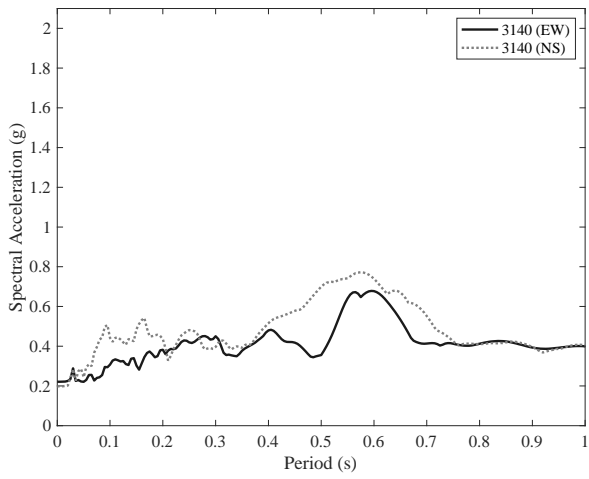
ID	DG (EMS-98)	6 February 2023	20 February 2023	Seismic index			
		Resultant PGA (g)		λ_{i1x}	λ_{i1y}	λ_{i2}	λ_o
C1	2	0.33	0.12	0.06	0.10	0.43	0.08
C2	4	0.33	0.12	0.04	0.13	0.28	0.11
C3	5	0.33	0.12	0.05	0.11	0.40	0.13
C4	5	0.33	0.12	0.06	0.10	0.47	0.06
C5	1	0.26	0.22	0.07	0.11	0.62	0.10
C6	4	0.26	0.22	0.03	0.11	0.33	0.11
C7	3	0.26	0.22	0.62	1.06	0.57	0.08
C8	4	0.54	0.33	1.08	0.39	0.54	0.09
C9	5	0.54	0.33	0.04	0.07	0.29	0.12
C10	2	0.33	0.12	0.69	0.96	0.50	0.10
M1	5	0.58	0.54	0.09	0.13	0.30	0.13
M2	1	0.42	0.54	1.13	0.79	0.44	0.11
M3	4	0.58	0.54	0.98	0.69	0.41	0.13
M5	3	0.19	0.04	0.71	0.54	1.20	0.12
M6	2	0.29	0.02	0.05	0.09	0.51	0.19
M7	1	0.20	0.01	0.77	0.75	0.75	0.14
M8	1	0.20	0.01	0.94	1.44	0.80	0.15
P1	3	0.66	0.54	0.07	0.14	0.20	0.06
P2	5	0.33	0.12	0.09	0.11	0.54	0.10
P3	3	0.19	0.04	n.a	n.a	n.a	n.a
P4	4	0.66	0.54	n.a	n.a	n.a	n.a
P5	3	0.33	0.12	n.a	n.a	n.a	n.a
P6	3	0.54	0.33	0.95	1.31	0.31	0.11
R1	4	0.58	0.54	0.06	0.20	0.16	0.07
R2	1	0.58	0.54	0.08	0.27	0.16	0.14
R3	1	0.26	0.22	n.a	n.a	n.a	n.a
R4	4	0.26	0.22	0.66	1.29	0.52	0.09
R5	3	0.26	0.22	0.05	0.06	0.69	0.03



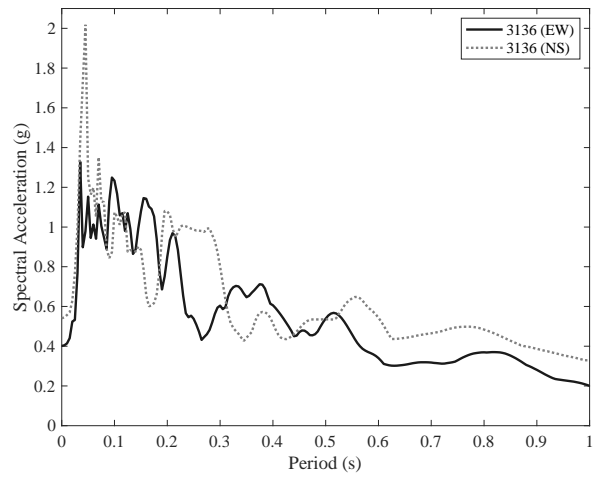
(a)



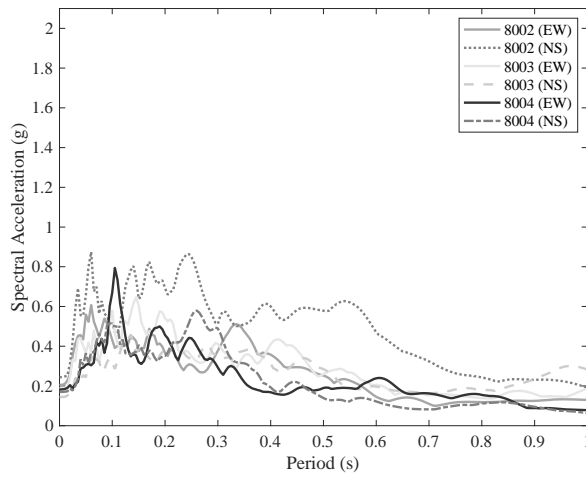
(b)



(c)



(d)



(e)

562
563

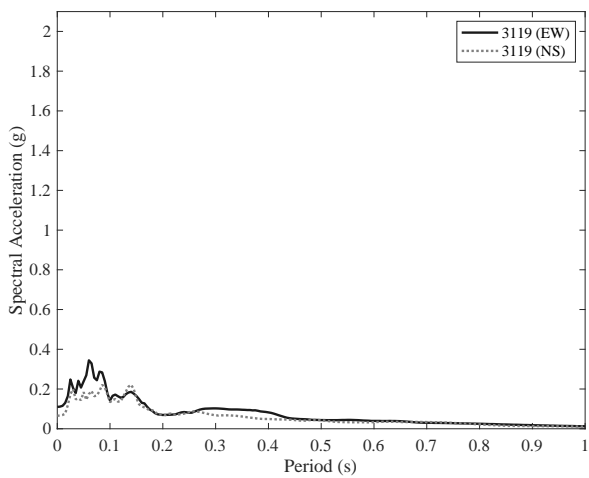
564
565

566

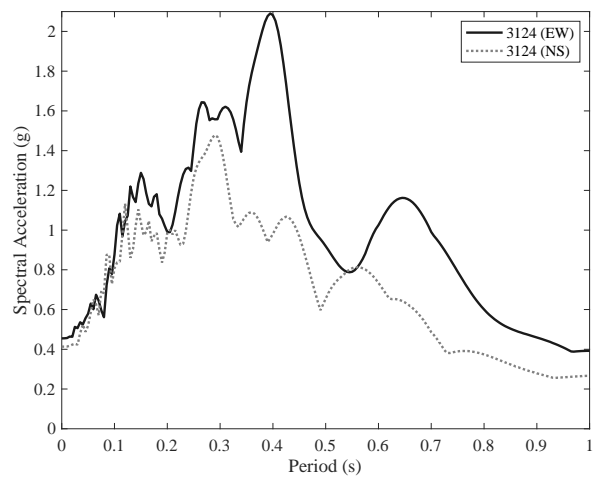
Fig.A1. Spectral acceleration of ground motion records used for the Pazarcık earthquake: a) İskenderun b) Antakya c) Samandağ

567

d) Altınözü e) Osmaniye

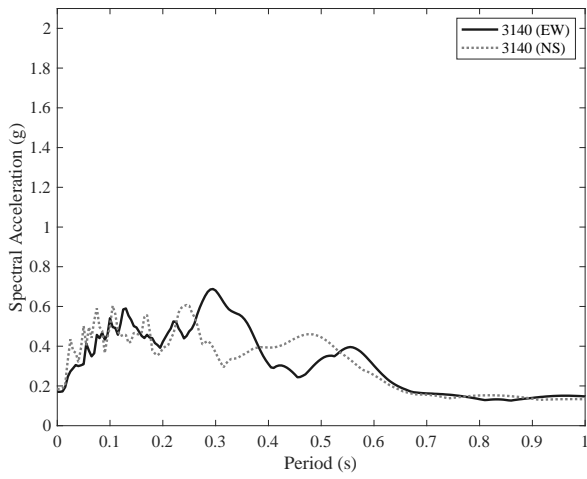


(a)

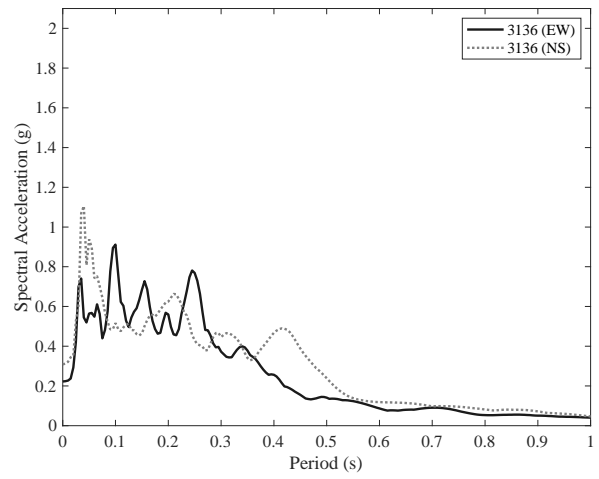


(b)

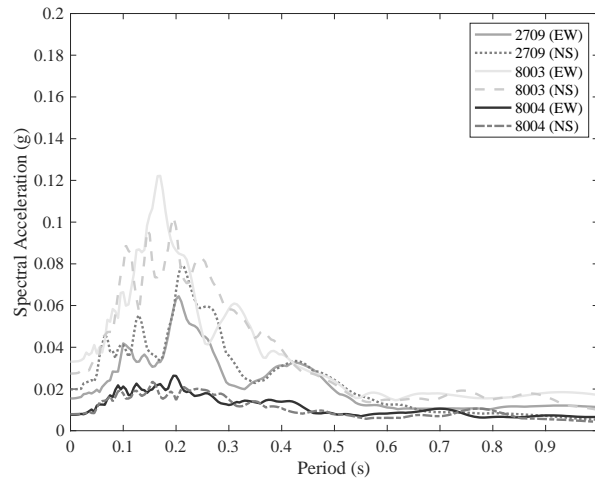
568
569



(c)



(d)



(e)

Fig.A2. Spectral acceleration of ground motion records used for the Samandağ earthquake: a) İskenderun b) Antakya c) Samandağ d) Altınözü e) Osmaniye

References

- Abrahamczyk L, Schwarz J, Langhammer T, Genes MC, Bikçe M, Kaçın S and Gülkan P (2013) Seismic risk assessment and mitigation in the Antakya–Maras region (SERAMAR): empirical studies on the basis of EMS-98. *Earthquake Spectra* 29(3): 683-704.
- AFAD (2023) Turkish Ministry of Interior Disaster and Emergency Management Presidency.
- Al-Shayea NA (2004) Effects of testing methods and conditions on the elastic properties of limestone rock. *Engineering GEOLOGY* 74(1-2): 139-156.
- ASCE/07-16 (2017) Minimum Design Loads and Associated Criteria for Buildings and Other Structures. *American Society of Civil Engineers, Virginia*.

- 587 Banerjee Basu S and Shinozuka M (2011) Effect of Ground Motion Directionality on Fragility Characteristics of a Highway
588 Bridge. *Advances in Civil Engineering* 2011: 536171.
- 589 Barnaure M and Cincu M (2020) Testing methods for the assessment of material properties in historical masonry structures: a
590 review. *IOP conference series: materials science and engineering*. IOP Publishing, 012003.
- 591 Borri A, Corradi M, Castori G and De Maria A (2015) A method for the analysis and classification of historic masonry. *Bulletin
592 of Earthquake Engineering* 13: 2647-2665.
- 593 Borri A, Corradi M and De Maria A (2020) The Failure of Masonry Walls by Disaggregation and the Masonry Quality Index.
594 *Heritage* 3(4): 1162-1198.
- 595 Brotons V, Tomás R, Ivorra S and Grediaga A (2014) Relationship between static and dynamic elastic modulus of calcarenite
596 heated at different temperatures: the San Julián's stone. *Bulletin of Engineering Geology and the Environment* 73: 791-799.
- 597 Çalik İ, Bayraktar A, Türker T and Karadeniz H (2020) Ambient vibration based-simplified frequency formulas for historical
598 masonry stone mosques with timber truss roofs. *Journal of Architectural Conservation* 26(3): 247-264.
- 599 Demir A (2016) *Çağlar İçinde Antakya (in Turkish)*. Dafne Kitap.
- 600 EERC (2023) *Preliminary Reconnaissance Report on February 6, 2023 Kahramanmaraş Pazarcık (Mw= .7) and Elbistan
601 (Mw=7.6) Earthquakes*. Middle East Technical University, Ankara.
- 602 Eissa EA and Kazi A (1988) Relation between static and dynamic Young's moduli of rocks. *International Journal of Rock
603 Mechanics and Mining Sciences* 25(6): 479-482.
- 604 Ferreira Pinto AP, Sena da Fonseca B and Vaz Silva D (2021) Mechanical characterization of historical rubble stone masonry
605 and its correlation with the masonry quality assessment. *Construction and Building Materials* 281: 122168.
- 606 Gambilongo L, Barontini A, Silva RA and Lourenço PB (2023) Evaluation of non-destructive techniques for mechanical
607 characterisation of earth-based mortars in masonry joints. *Construction and Building Materials* 392: 131960.
- 608 Garbioğlu Ö (2017) *Tanzimat'tan Cumhuriyet'e Hatay'daki Kamu Yapıları. Master's Thesis (in Turkish)*. Mimar Sinan Fine Art
609 University.
- 610 Gardner G, Gardner L and Gregory A (1974) Formation velocity and density—The diagnostic basics for stratigraphic traps.
611 *Geophysics* 39(6): 770-780.
- 612 Geneş MC, Abrahamczyk L, Kaçın S and Erberik MA (2017) Yığma yapıların deprem etkisi altında gözleme ve hesaba bağlı
613 değerlendirilmesi için yöntem (in Turkish). In: *4.UDMSK*.
- 614 Ghiassi B, Vermelfoort AT and Lourenço PB (2019) Chapter 7 - Masonry mechanical properties. In: Ghiassi B and Milani G
615 (eds) *Numerical Modeling of Masonry and Historical Structures*. Woodhead Publishing, pp.239-261.
- 616 Gonen S and Soyoz S (2021) Investigations on the elasticity modulus of stone masonry. *Structures*. Elsevier, 378-389.
- 617 Grünthal G and Levret A (1998) European macroseismic scale 1998 (EMS-98) cahiers du centre Européen de géodynamique et
618 de séismologie 15. *Centre Européen de géodynamique et de séismologie, Luxembourg*.

619 Günaydin M, Genç AF, Altunışık AC, Hacıfendioglu K, Okur FY, Okur E and Adanur S (2022) Structural condition assessment
620 of a historical masonry school building using experimental and numerical methods. *Journal of Civil Structural Health*
621 *Monitoring* 12(5): 1083-1113.

622 Housner GW (1963) The behavior of inverted pendulum structures during earthquakes. *Bulletin of the Seismological Society of*
623 *America* 53(2): 403-417.

624 Karabacak V, Özkaymak Ç, Sözbilir H, Tatar O, Aktuğ B, Özdağ ÖC, Çakir R, Aksoy E, Koçbulut F and Softa M (2023) The
625 2023 Pazarcık (Kahramanmaraş, Türkiye) earthquake (Mw 7.7): implications for surface rupture dynamics along the East
626 Anatolian Fault Zone. The Geological Society of London, jgs2023-2020.

627 Kocáb D, Misák P and Cikrle P (2019) Characteristic curve and its use in determining the compressive strength of concrete by
628 the rebound hammer test. *Materials* 12(17): 2705.

629 Kumavat HR, Chandak NR and Patil IT (2021) Factors influencing the performance of rebound hammer used for non-destructive
630 testing of concrete members: A review. *Case Studies in Construction Materials* 14: e00491.

631 Li H, Yang S-Q, Yang Z, Zhou X-P, Tian W-L and Wang S-S (2023) Experimental and numerical study on the mechanical
632 behaviors and crack propagation of sandstone containing two parallel fissures. *Theoretical and Applied Fracture Mechanics*
633 126: 103965.

634 Liberatore D, Masini N, Sorrentino L, Racina V, Sileo M, AlShawa O and Frezza L (2016) Static penetration test for historical
635 masonry mortar. *Construction and Building Materials* 122: 810-822.

636 Lopez S, D'Amato M, Ramos L, Laterza M and Lourenço PB (2019) Simplified formulations for estimating the main frequencies
637 of ancient masonry churches. *Frontiers in Built Environment* 5: 18.

638 Lourenço PB, Oliveira DV, Leite JC, Ingham JM, Modena C and da Porto F (2013) Simplified indexes for the seismic assessment
639 of masonry buildings: International database and validation. *Engineering Failure Analysis* 34: 585-605.

640 Lourenço PB and Roque JA (2006) Simplified indexes for the seismic vulnerability of ancient masonry buildings. *Construction*
641 *and Building Materials* 20(4): 200-208.

642 Maccarini H, Vasconcelos G, Rodrigues H, Ortega J and Lourenço PB (2018) Out-of-plane behavior of stone masonry walls:
643 Experimental and numerical analysis. *Construction and Building Materials* 179: 430-452.

644 Marazzani J, Cavalagli N and Gusella V (2021) Elastic properties estimation of masonry walls through the propagation of elastic
645 waves: An experimental investigation. *Applied Sciences* 11(19): 9091.

646 Mavroulis S, Andreidakis E, Spyrou N-I, Antoniou V, Skourtsos E, Papadimitriou P, Kassaras I, Kaviris G, Tselentis GA,
647 Voulgaris N, Carydis P and Lekkas E (2019) UAV and GIS based rapid earthquake-induced building damage assessment
648 and methodology for EMS-98 isoseismal map drawing: The June 12, 2017 Mw 6.3 Lesvos (Northeastern Aegean, Greece)
649 earthquake. *International Journal of Disaster Risk Reduction* 37: 101169.

650 Meli R (1994) Structural design of masonry buildings: The Mexican practice. *Special Publication* 147: 239-262.

651 NCSE-2002 (2002) Norma de Construcció n Sismorresistente. Parte General y Edificaci3n (Spanish Standard). *Ministerio de*
652 *Fomento*.

653 NTC-2008 (2008) Norme Tecniche per le Costruzioni. *S.O. n. 30 of the Official Gazette of the Italian Republic*.

654 NZSEE (2006) Assessment and Improvement of the Structural Performance of Buildings in Earthquakes. *New Zealand Society*
655 *for Earthquake Engineering*.

656 Ozturk M, Arslan MH and Korkmaz HH (2023) Effect on RC buildings of 6 February 2023 Turkey earthquake doublets and
657 new doctrines for seismic design. *Engineering Failure Analysis* 153: 107521.

658 3ver S, B3yüksaraç A, Bekta 3 and Filazi A (2011) Assessment of potential seismic hazard and site effect in Antakya (Hatay
659 Province), SE Turkey. *Environmental Earth Sciences* 62(2): 313-326.

660 Sagbas G, Sheikhi Garjan R, Sarikaya K and Deniz D (2023) Field reconnaissance on seismic performance and functionality of
661 Turkish industrial facilities affected by the 2023 Kahramanmaraş earthquake sequence. *Bulletin of Earthquake Engineering*.

662 Sancı F (2006) *Hatay İlinde Türk Mimarisi I. Doctoral Thesis (in Turkish)*. Ankara University.

663 Standardization ECf (2005) *Eurocode 6: Design of Masonry Structures – Part 1-1: General rules for reinforced and unreinforced*
664 *masonry structures*.

665 Sürmeli BS (2019) *Hatay Musa Dağı kırsal yerleşimleri ve geleneksel konutların korunması için öneriler. Master's Thesis (in*
666 *Turkish)*. Istanbul Technical University.

667 Szabó S, Funari MF and Lourenço PB (2023) Masonry patterns' influence on the damage assessment of URM walls: Current
668 and future trends. *Developments in the Built Environment* 13: 100119.

669 TAÇDAM (2023) *Antakya'nın Çok Katmanlı Kültürel Mirasının Deprem Sonrası Belgelemesi, Hasar Tespiti ve*
670 *Değerlendirilmesi (in Turkish)*. Middle East Technical University, Ankara.

671 Taftoglou M, Valkaniotis S, Papathanassiou G and Karantanellis E (2023) Satellite Imagery for Rapid Detection of Liquefaction
672 Surface Manifestations: The Case Study of Türkiye–Syria 2023 Earthquakes. *Remote Sensing* 15(17): 4190.

673 TBEC (2018) Turkish Building Earthquake Code. *Turkish Ministry of Interior Disaster and Emergency Management Presidency,*
674 *Ankara*.

675 USGS (2023) U.S. Geological Survey. *Earthquake Lists, Maps, and Statistics, accessed July 13, 2023 at URL*
676 <https://www.usgs.gov/natural-hazards/earthquake-hazards/lists-maps-and-statistics>.

677 Viles H, Goudie A, Grab S and Lalley J (2011) The use of the Schmidt Hammer and Equotip for rock hardness assessment in
678 geomorphology and heritage science: a comparative analysis. *Earth Surface Processes and Landforms* 36(3): 320-333.

679 Wang X, Cheng Z, Zhou Y, Xu K and Liao Y (2024) Study on microscopic failure mechanism and numerical simulation of
680 sandstone under different saturated pressure. *Unconventional Resources* 4: 100058.

681 Wróblewska J, Kowalski R, Głowacki M and Juchnowicz-Bierbasz B (2021) Application of ultrasonic pulse velocity test to
682 concrete assessment in structures after fire. *Archives of Civil Engineering* 67(3): 395-413.

- 683 Žalský J, Vokáč M, Hrabánek M and Hurtig K (2023) Development of a New Nondestructive Method for the In-Situ
684 Determination of Mortar Strength. *Buildings* 13(2): 273.
- 685